Schweizerische Eidgenossenschaft
Confédération suisse
Confederazione Svizzera
Confederaziun svizra

Federal Department of the Environment,
Transport, Energy and Communications DETEC

Swiss Federal Office of Energy
Energy Research and Cleantech

Final report from 5 August 2024

HYTMOB

Hydrogen Tank for Mobility

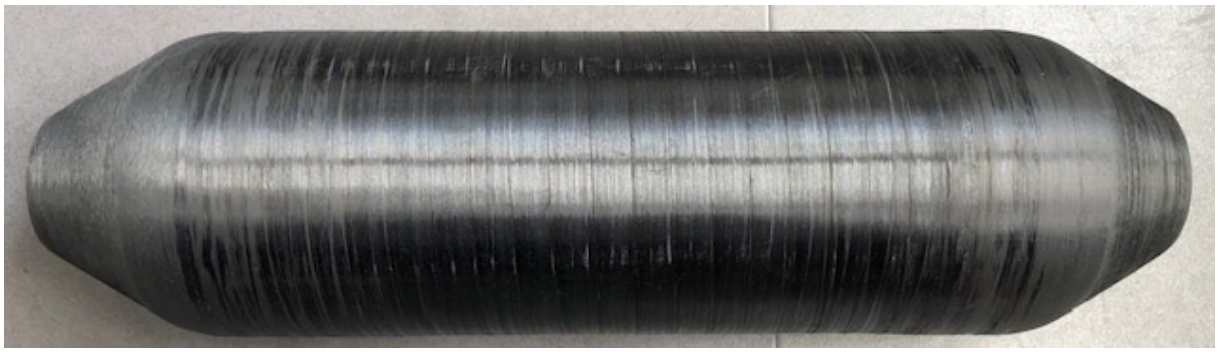

Source: ©NGT, 2024

Publisher:
Swiss Federal Office of Energy SFOE
Energy Research and Cleantech
CH-3003 Berne
www.energy-research.ch

Subsidy recipients:
HEIG-VD Institut COMATEC
Route de Cheseaux 1, 1401 Yverdon-les-Bains
https://heig-vd.ch/recherche/instituts/comatec/

HEIA-FR, Institut iRAP
Passage du Cardinal 1, bâtiment A, 1700 Fribourg
https://www.heia-fr.ch/fr/recherche-appliquee/instituts/irap/

New Generation Tanks SA
Route des Martines 101, 1052 Le Mont-Sur-Lausanne
https://newgenerationtanks.com/

Autors:
Joël Cugnoni, HEIG-VD Comatec, joel.cugnoni@heig-vd.ch
Bruno Bürgisser, HEIA-FR iRAP, bruno.buergisser@hefr.ch
Gilles Rocher, NGT, contact@newgenerationtanks.com

SFOE project coordinator:
Stefan Oberholzer, stefan.oberholzer@bfe.admin.ch

SFOE contract number: SI/502438-01

Summary

In the current context of decarbonizing the economy to reduce greenhouse gas emissions and limit global warming, hydrogen produced from decarbonized electricity is a particularly interesting energy carrier for decarbonizing industry and transportation. However, its storage on board fuel cell vehicles and its transport to distribution points remain challenging. Compressed hydrogen tanks are heavy, difficult to integrate into vehicles, made of non-recyclable materials, and produced through an inefficient manufacturing process. To meet the sector's needs, New Generation Tanks (NGT) is developing ultralight, conformable tanks made from recyclable materials using a manufacturing process with high productivity potential.

The goal of the HYTMOB project was to raise the technological maturity of NGT tanks from level 4 to level 5 and to enable all project partners to develop an understanding of the issues related to high-pressure gas storage, particularly from the perspective of the materials used and their processing.

The project was organized into seven work packages covering the project's needs in modeling, manufacturing, and characterization. The three project partners were able to utilize and deepen their expertise, develop tools and methodologies, and create real know-how that they can rely on for future projects.

The project's objectives were exceeded as tanks with performance superior to the target were produced, with various materials, meeting the needs of the initially envisaged application as well as other applications.

Zusammenfassung

Im aktuellen Kontext der Dekarbonisierung der Wirtschaft, um Treibhausgasemissionen zu reduzieren und die globale Erwärmung zu begrenzen, ist Wasserstoff, der aus dekarbonisiertem Strom produziert wird, ein besonders interessanter Energieträger zur Dekarbonisierung der Industrie und des Transports. Seine Speicherung in Brennstoffzellenfahrzeugen und der Transport zu Verteilungspunkten bleiben jedoch eine Herausforderung. Komprimierte Wasserstofftanks sind schwer, aber auch schwierig in Fahrzeuge zu integrieren, aus nicht recycelbaren Materialien gefertigt und durch ein ineffizientes Herstellungsverfahren produziert. Um den Bedürfnissen des Sektors gerecht zu werden, entwickelt New Generation Tanks (NGT) ultraleichte, anpassungsfähige Tanks aus recycelbaren Materialien mit einem Verfahren, dessen Produktivitätspotenzial sehr gross ist.

Ziel des HYTMOB-Projekts war es, die technologische Reife der NGT-Tanks von Stufe 4 auf Stufe 5 zu erhöhen und allen Projektpartnern zu ermöglichen, ein Verständnis für die Probleme im Zusammenhang mit der Hochdruckgaslagerung zu entwickeln, insbesondere aus der Perspektive der verwendeten Materialien und deren Umsetzung.

Das Projekt war in sieben Arbeitspakete unterteilt, die die Anforderungen des Projekts in Modellierung, Fertigung und Charakterisierung abdeckten. Die drei Projektpartner konnten ihre Expertise nutzen und vertiefen, Werkzeuge und Methodologien entwickeln und ein echtes Know-how schaffen, auf das sie bei zukünftigen Projekten zurückgreifen können.

Die Projektziele wurden übertroffen, da Wasserstofftanks mit Leistungen über den Zielvorgaben hergestellt werden konnten, dies ausserdem, mit verschiedenen Materialien und um den Anforderungen der ursprünglich geplanten Pilotanwendung sowie anderer Anwendungen gerecht zu werden.

Résumé

Dans le contexte actuel de décarbonation de l'économie pour réduire les émissions de gaz à effet de serre et limiter le réchauffement climatique, l'hydrogène produit à partir d'électricité décarbonée est un vecteur énergétique particulièrement intéressant pour réduire l'utilisation d'hydrocarbures dans l'industrie et les transports. Son stockage à bord de véhicules à piles à hydrogène et son transport jusqu'aux points de distribution restent un défi. Les réservoirs d'hydrogène comprimés sont lourds, difficiles à intégrer dans les véhicules, faits de matériaux non-recyclables par un procédé de fabrication peu efficace. Pour répondre aux besoins du secteur, New Generation Tanks (NGT) développe des réservoirs ultralégers, conformables et faits de matériaux recyclables par un procédé à haut potentiel de productivité.

L'objectif du projet HYTMOB était d'élever la maturité technologique des réservoirs NGT du niveau 4 au niveau 5 et de permettre à tous les partenaires du projet de développer une compréhension des problèmes liés au stockage de gaz à haute pression, en particulier du point de vue des matériaux utilisés et de leur mise en œuvre.

Le projet a été organisé en 7 work packages couvrant les besoins du projet en modélisation, fabrication et caractérisation. Les trois partenaires du projet ont pu utiliser et approfondir leur expertise, développer des outils et méthodologies et créer un réel savoir-faire sur lesquels ils pourront s'appuyer pour de futurs projets.

Les objectifs du projet ont été dépassés puisque des réservoirs avec des performances supérieurs aux performances cibles ont été réalisés, avec plusieurs matières et pour répondre aux besoins de l'application envisagée initialement mais aussi d'autres applications.

Main findings («Take-Home Messages»)

- Material processability is critical: work performed before HYTMOB (especially within the POSSHYS project) allowed for the identification of the best polymer candidates for hydrogen storage, based on their intrinsic properties. However, HYTMOB has revealed how critical polymer processability is for their final performance and compatibility with compressed hydrogen storage.
- Several polymers can be considered for compressed hydrogen storage. Each of them has its specific design and processing window, leading to its use in specific applications.
- The technology supported by HYTMOB will not only enable the creation of efficient pressure tanks for fuel cell vehicles but also for other applications such as hydrogen transport by tube trailer and Multiple Element Gas Containers.
- The technology supported by HYTMOB opens a new era for pressure tanks, based on a new paradigm compared to the past 70 years of composite pressure tank design and manufacturing.

Contents

List of abbreviations

AFP	Automated Fibre Placement (possibly with In-Situ consolidation)
COMATEC	Institut de Conception mécanique et Technologies des matériaux
FEA	Finite Element Analysis
iRAP	Institute for Applied Plastic Research
NGT	New Generation Tanks SA
MEGC	Multiple Element Gas Containers
POSSHYS	Polymer Screening and Selection for Hydrogen Storage (previous project)
SFOE	Swiss Federal Office of Energy

1 Introduction

1.1 Initial situation and background

The storage of hydrogen poses a major challenge due to its very low volumetric density of just 0.083 kg/m³ at atmospheric pressure. In order to achieve suitable storage densities for mobility applications, hydrogen typically has to be compressed to several hundred bars (typically 350 bar for lorry or bus applications and 700 bar for passenger cars). The storage tanks must be as light as possible to ensure that the storage density of the overall storage system is sufficiently high.

State-of-the-art hydrogen pressure tanks used for mobility applications, known as type 4 pressure tanks, are made of a thermoplastic polymer liner and a carbon fibre reinforced thermoset polymer outer structure. Manufactured by filament winding, these tanks are much lighter than their metal counterparts and are well suited to mobility applications. However, such tanks suffer from a number of limitations:

- production requires a considerable amount of expensive carbon fibres;
- tanks are typically not recyclable;
- they are bulky and difficult to integrate into vehicles; and
- they are produced using an outdated, capital-intensive multi-step process.

Not many companies in the value chain are focussing on hydrogen tanks and the fuel cell vehicle industry is currently bound to use these pressure tanks but would welcome better solutions. The hydrogen storage technology developed by NGT allows for the reduction of the amount of carbon fibres used in pressure tanks and for the cost-effective replacement of non-recyclable epoxy by recyclable thermoplastic polymers. It also enables the production of slender pressure tanks from a high-efficiency semi-continuous manufacturing process that can easily fit into a vehicle floor or chassis. However, this technology needs further development to reach a maturity level compatible with market expectations.

NGT employs an extrusion process to produce thermoplastic liners. Automatic fibre placement with in-situ consolidation is used for a longitudinal reinforcement layer of carbon fibres pre-impregnated with the same thermoplastic polymer as the liner. The ends are subsequently closed and the same prepreg is wound circumferentially to complete the tank. Unlike conventional Type IV tanks, NGT tanks have one end with a progressively decreasing diameter. This design offers a better solution for exploiting the potential of carbon fibres in terms of tensile strength, and the continuity between liner and matrix material opens up the possibility of recycling.

1.2 Motivation of the project

When the project HYTMOB started in summer 2022, NGT's technology was at TRL4: a simple prototyping equipment using hot air to process thermoplastic prepreg tape had been developed, and proof-of-concept prototypes made of glass fibre reinforced polypropylene liners were tested to a burst pressure of 230 bar. The laboratory "Comatec" (Institut de Conception mécanique et Technologies des matériaux) at HEIG-VD had developed a first model to design and simulate NGT prototypes (thanks to InnoChèque No. 32104.1 INNO-EE) based on simple assumptions and basic Finite Element Analysis meshing. Comatec and NGT had also worked together within the POSSHYS project (Polymer Screening and Selection for Hydrogen Storage, https://www.aramis.admin.ch/Grunddaten/?ProjectID=47508) supported by SFOE, during which nearly 20 thermoplastic polymers were evaluated, and two polymers were finally identified as the most promising candidates for hydrogen storage, based essentially on their intrinsic properties.

1.3 Project objectives

The primary objective of the HYTMOB project was to advance the technology from TRL4 to TRL5 by using the polymer identified within the POSSHYS project in 2021 to create pressure tank prototypes matching the technical specifications for hydrogen bicycles and scooters, including a burst pressure above 800 bar. Other objectives included developing a deep understanding of the compressed hydrogen storage challenge, and building tools and methods for the characterization and processing of materials suitable for compressed hydrogen storage and transport.

2 Approach and method

An extended range of expertise in different fields was necessary to achieve the objectives. The project was broken down into 7 work packages and 8 sub-work packages, each led by experts:

- WP1: Pressure tank design and simulation
    - WP1.1: Design of the metal insert – led by Comatec
    - WP1.2: Design and simulation of the entire pressure tank – led by Comatec
- WP2: Design and manufacturing of the liner
    - WP2.1: End part injection simulation and injection mould conception – led by iRAP
    - WP2.2: Injection mould and metal insert manufacturing – led by iRAP & NGT
    - WP2.3: Injection of the end-part – led by iRAP
    - WP2.4: Liner assembly – led by NGT
- WP3: Materials characterization – led by Comatec
- WP4: Manufacturing of the composite structure – led by NGT
- WP5: Standards analysis and pressure tanks testing – led by NGT
    - WP5.1: Standard analysis
    - WP5.2Pressure tanks testing
- WP6: Pressure tanks recyclability assessment – led by iRAP
- WP7: Project coordination and communication – led by NGT

At the start of the project, it was anticipated that 2 design–manufacturing–testing loops would be necessary to reach the objectives as shown in the figure 1 below:

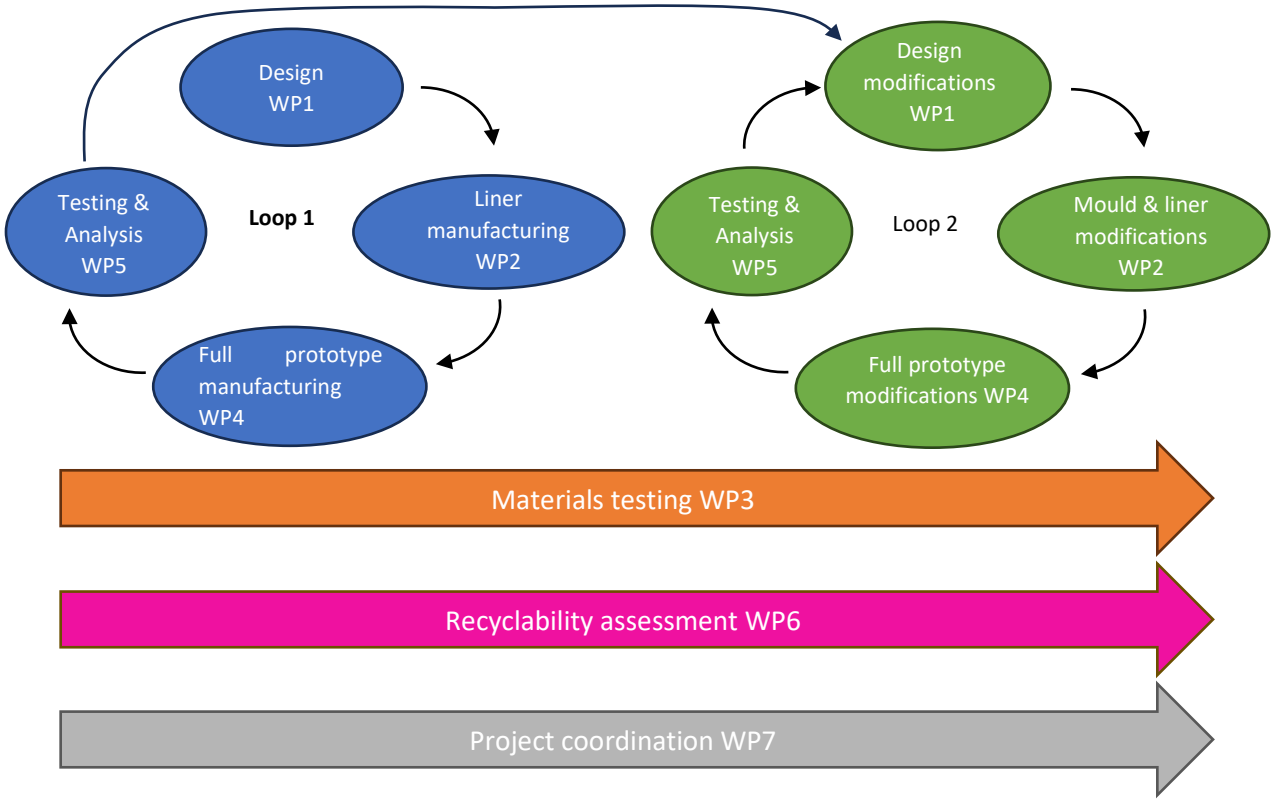

Figure 1: Project structure diagram

The Work packages 3, 6, and 7 (materials testing, recyclability assessment, and project coordination, respectively) could be conducted in parallel with the 2 loops of design–manufacturing–testing. The results of WP3 (materials characterization) also fed into WP1.2 and were used to design or adjust the design of the pressure tank prototypes.

Ultimately, after the discovery of a number of unexpected challenges, 3 loops were necessary to achieve and even surpass the initial goals.

3 Description of the plant/experimental setup

Several pieces of equipment or experimental setups have been used and possibly developed within the HYTMOB framework.

WP1.2 consisted in the develop and refinement of a parametric FEA model to simulate the behaviour of tank prototypes under pressure, depending on their design and material. Figure 2 below shows the level of stress in the metal insert, in the liner and in the composite structure when an internal pressure of 800 bar is applied to the tank prototype.

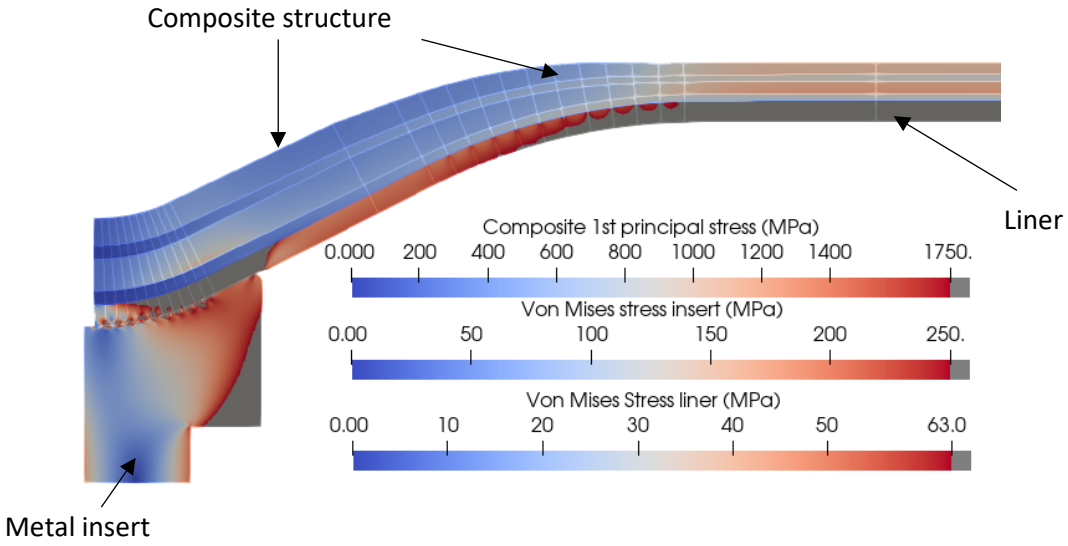

Figure 2: Representation of the stress level on the pressure tank's metal insert, liner and composite structure resulting from an internal pressure of 800 bar for a given geometry

This parametric model has allowed for the evaluation of numerous configurations with different geometries, materials, layer organizations, thicknesses, etc. It has also been used to precisely design and manufacture the metal insert (WP1.1 & 2.2). Figure 3 below shows the design of the metal insert obtained after loop 1 and the corresponding machined part:

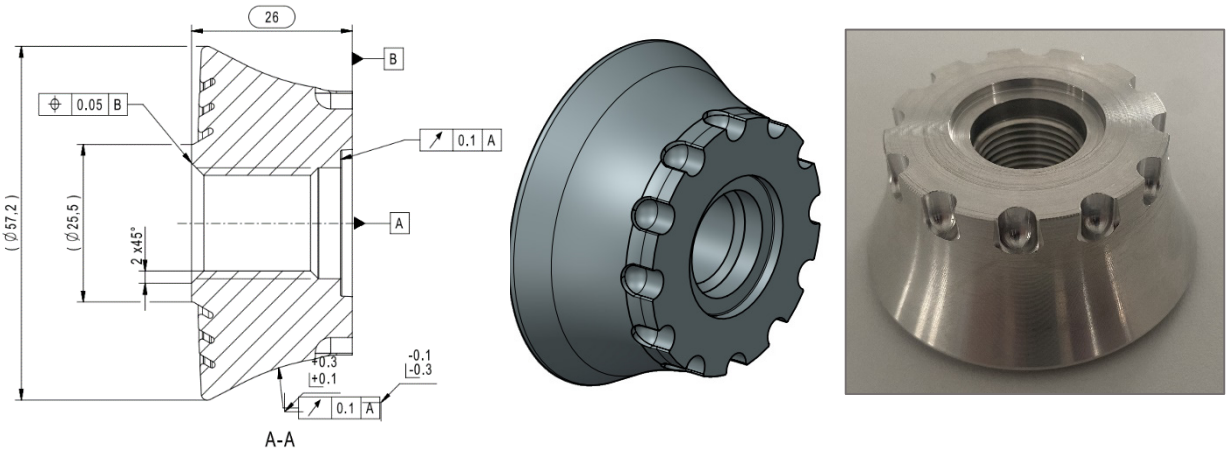

Figure 3: Designed (left and center) and machined (right) metal insert after loop 1

Once the metal insert geometry was defined, the liner was designed and built around it, dividing the entire liner into 4 sections. These sections could be manufactured using injection moulding in a small and affordable mould. Figure 4 below shows the liner's end-part and complete liner

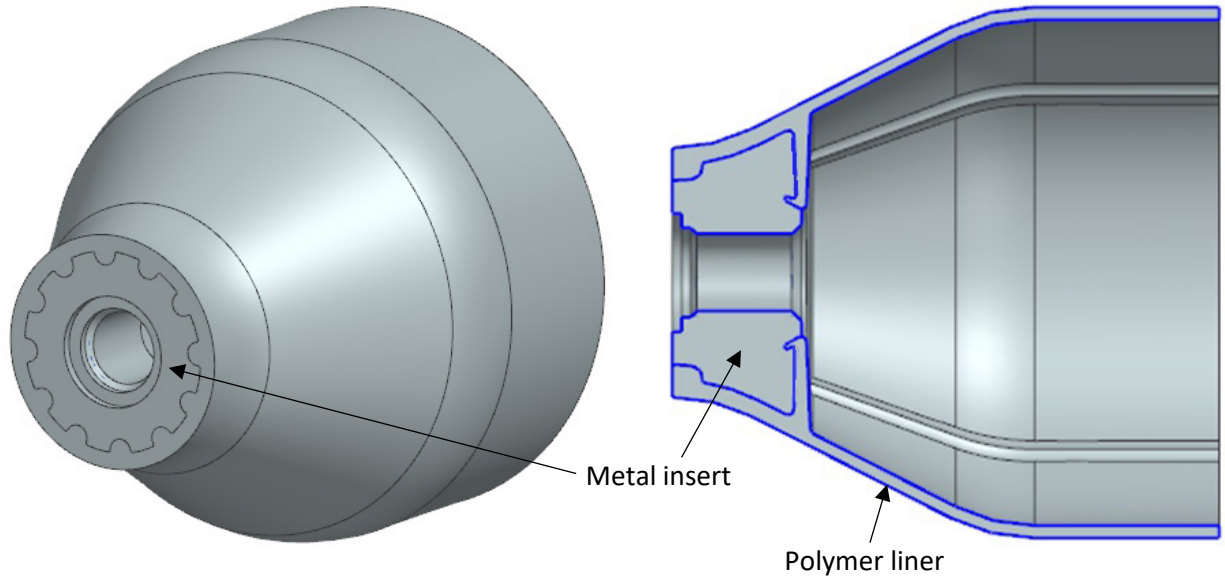

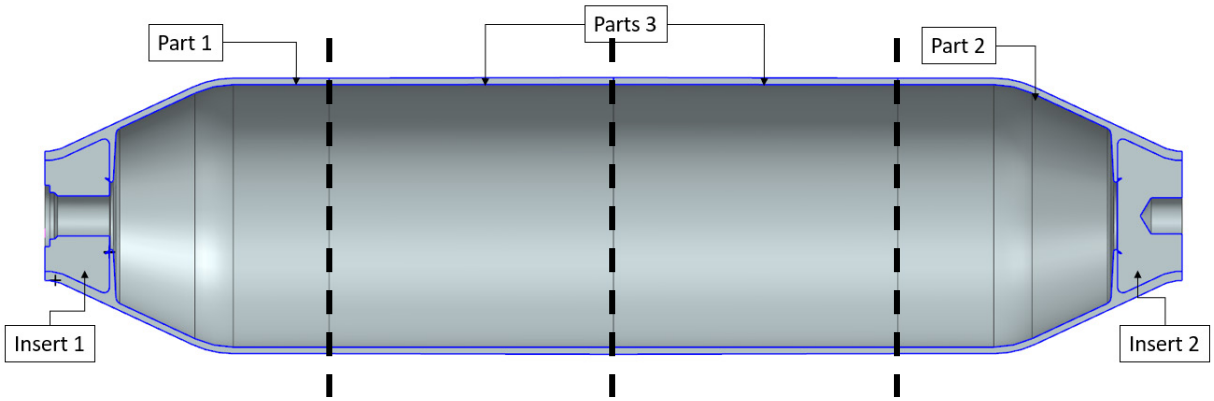

Figure 4: 3D view of the end-part (top left), cross section of the end-part (top right) and complete liner made of 4 components: 2 end-parts with different metal inserts (inlet on the left and bottom on the right) and 2 tubular sections in the middle

It was then necessary to simulate the injection of the end part with polymer A, identified at the end of the POSSHYS project, to ensure that the defined geometry could be successfully produced by injection with polymer A (WP 2.1). Figure 5 is an example of injection simulation results.

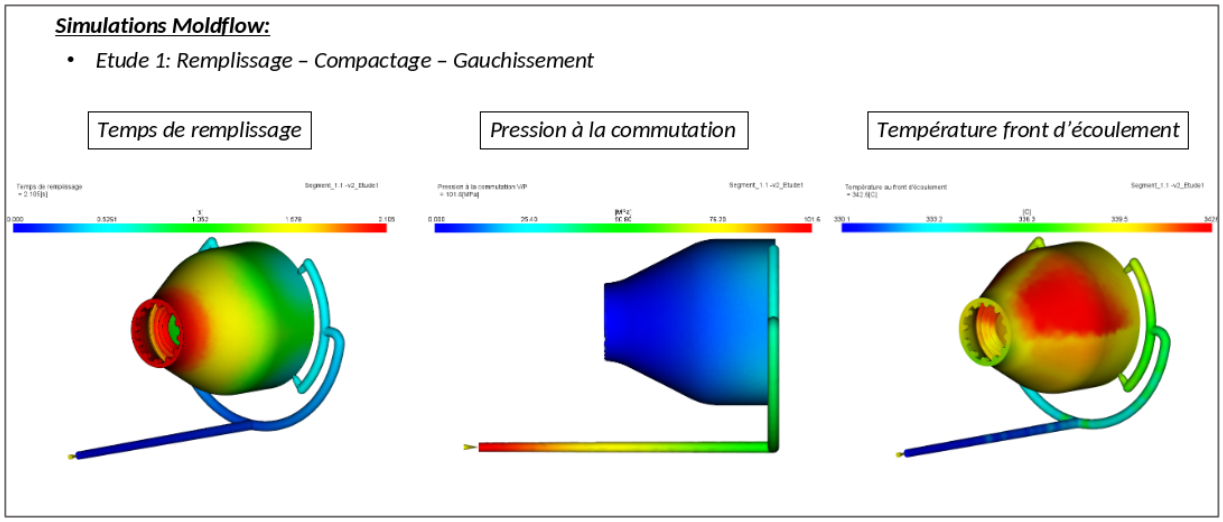

Figure 5: Simulation of the Injection Moulding Process (Rheological study by Moldflow) of the defined end-part geometry. Determination of the necessary injection parameters: filling time, injection pressure and loss of the melt during the filling

Several iterations were made from the metal insert and liner design to the injection simulation until the injectability with Polymer A was optimized. Once this was achieved, the injection mould was conceived and designed as shown in figure 6 below.

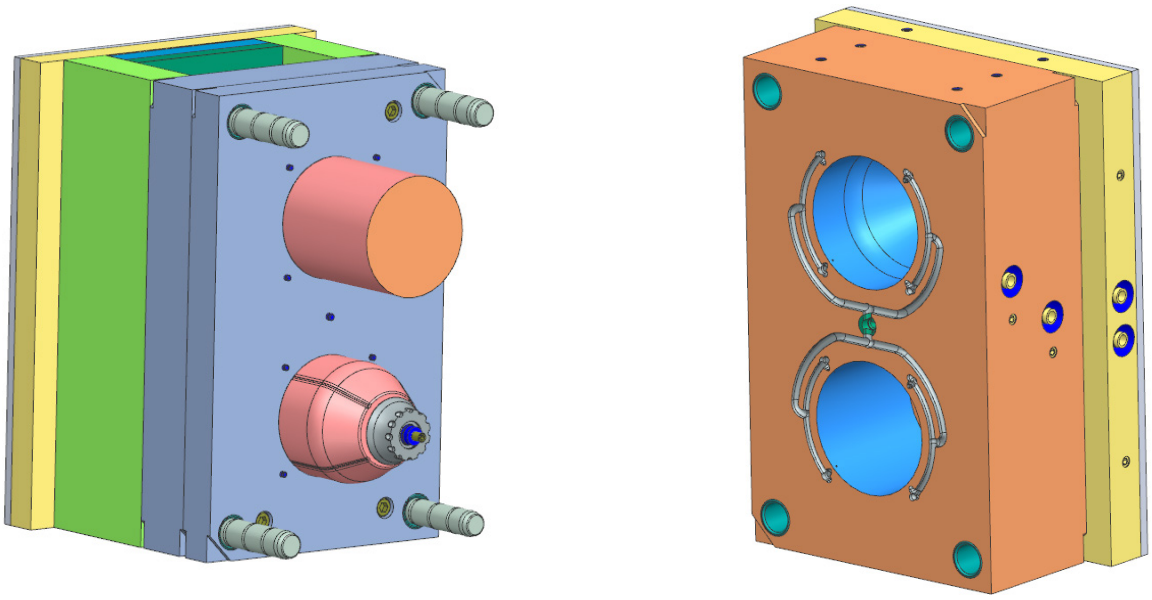

Figure 6: Conception of the injection mould with ejection side (left) and injection side (right)

Quotes were obtained from several mould manufacturers. The best offer was selected, and the mould was ordered and manufactured (WP 2.2). Once the mould was completed, the manufacturer conducted injection trials and produced a set of parts using Polymer A, which was sourced from the supplier (WP 2.3). Figure 7 below shows the mould in a batch of injected end-parts.

Figure 7: Mould mounted into the injection press, viewed behind the safety screen (left) and batch of end-parts injected with polymer A (right)

WP2.4 involved assembling the end-parts and tubular sections to create complete liners. Three welding technologies were tested to ensure proper assembly, including hot plate welding, hot air gun welding, and spin welding. Spin welding was identified as the most suitable technology, given the high melting point of Polymer A and the circular cross-section of the parts. It was necessary to machine welding profiles into the part sections to enhance the strength of the weld line. Several welding profiles (V, L, Z shapes – figure 8) were tested in combination with various welding parameters (rotation speed, friction duration, friction and contact pressure, etc.) as part of an experimental plan.

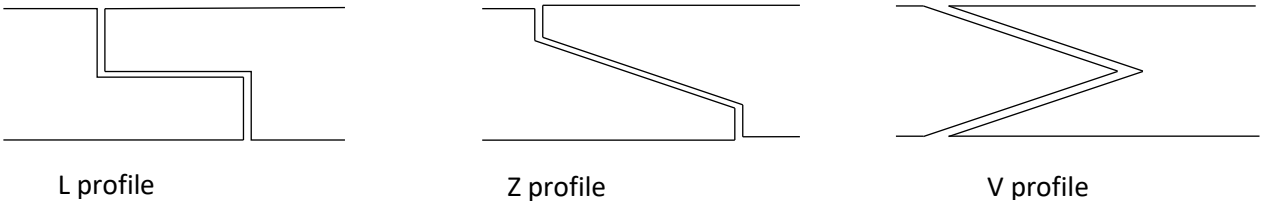

Figure 8: L, Z, V welding profiles (top) and fixtures developed to hold the part, machine the welding profiles and perform spin welding

Water tightness test setup developed to evaluate the performance of welding assembly

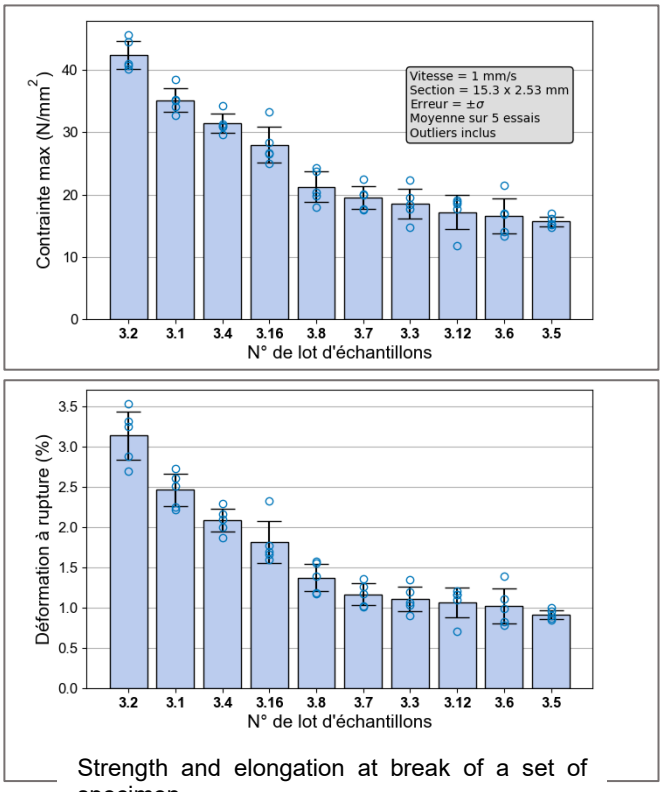

Strength and elongation at break of a set of specimen

Tensile test setup

Figure 9: Water tightness test applied on two tubular sections assembled by welding (top) and tensile test of specimen cut from two tubular sections assembled by welding (top)

Before assembling the full liners, the weld line resistance was tested using a specifically developed water tightness test and tensile strength measurements on samples cut from tubular sections assembled by welding. Figure 9 shows the water tightness fixtures and tensile test bench and results.

Liners have been assembled in accordance with the best performing configuration (WP2.4):

Although extensive work was done to identify and apply the optimal welding profiles and parameters, the weld line performance remained inconsistent and difficult to reproduce. Consequently, the liner thickness was increased during design–manufacturing–testing loop 2, and the mold was modified accordingly. Additionally, Polymer A was found to exhibit significant shrinkage, which created stress concentrations around the metal inserts. Combined with the polymer's relatively low elongation at break, this led to the formation of cracks around the metal insert (figure 10), resulting in loss of tightness.

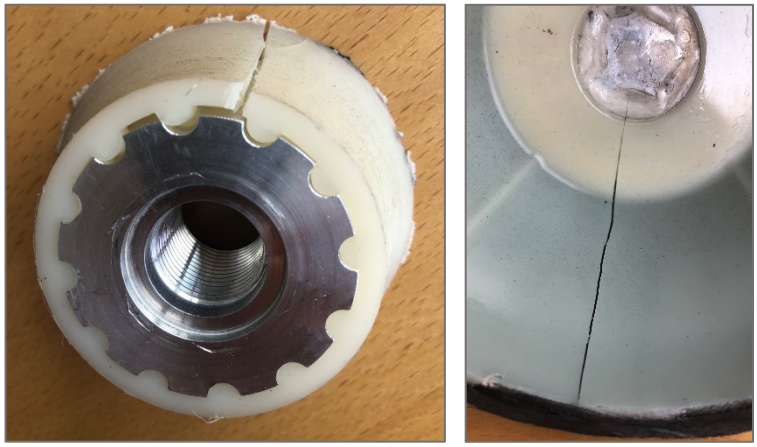

Figure 10: Complete liner assembled by welding (left) and crack appearing in the liner around the metal insert because of the high thermal shrinkage of polymer A

Work Package 4 – Manufacturing of the Composite Structure – involved significant modifications to the machine used to process the carbon fibre tape pre-impregnated with thermoplastic polymer (TP prepreg tape). This prototype machine was designed to lay the TP tape onto the liner to reinforce it while heating it above the polymer's melting temperature to ensure proper bonding of the tape to the liner or previous layers of tape.

Initially, a hot air gun was used for heating the tape. While this heating technology was effective for polypropylene tape, it was insufficient for processing tapes with higher melting temperatures at speeds suitable for manufacturing pressure tank prototypes. Consequently, an alternative heating source was implemented, increasing the tape deposition speed from a few millimeters per second for polypropylene to several tens of millimeters per second for Polymer A.

Due to the change in heating source and the increase in deposition speed, it was also necessary to upgrade the machine’s electric motors and automation system. Other components, such as the tape guiding line and compaction rolls, were modified or replaced, with only some parts of the machine chassis remaining unchanged. Additionally, the machine dimensions were increased to accommodate the manufacturing of more than one pressure tank prototype or longer prototypes in the future. Figure 11 show the machine at the start and at the end of the project.

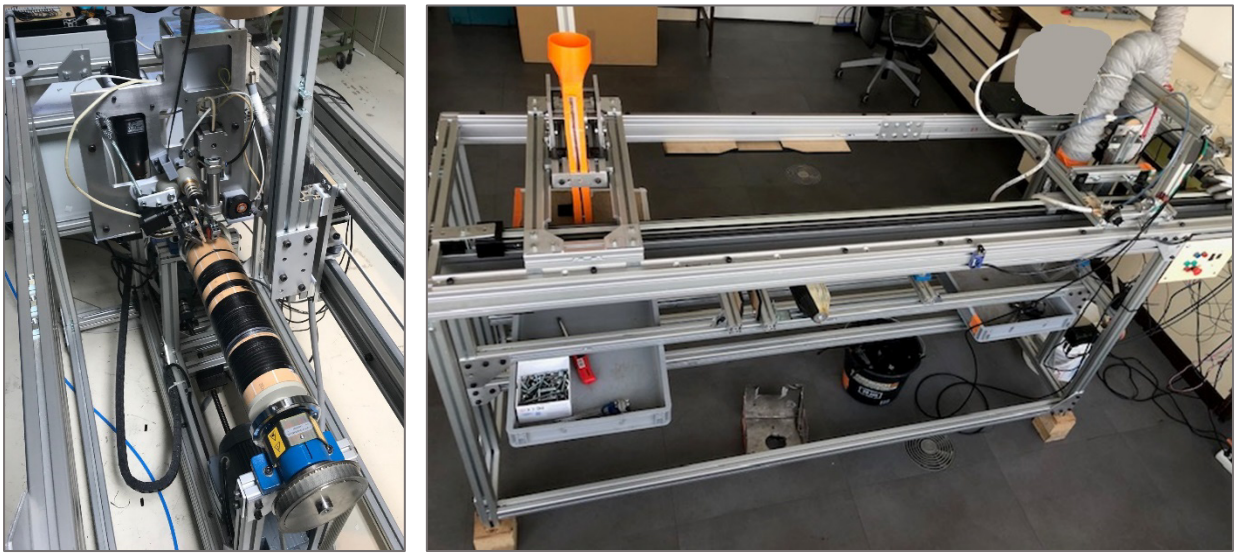

Figure 11: Initial prototype machine with hot air heating (left) and modified machine with a more powerful heating source, upgraded motors and automation, increased dimension and a deposition head specialized for longitudinal layers of tape and a deposition head specialized for hoop layers of tape (right)

The machine was then used and fine-tuned to process the TP tape and apply it to the liners. The specific grade of Polymer A used by the tape supplier for impregnating the carbon fibre filaments (a low viscosity grade to facilitate fibre impregnation) differed from the grade provided by another supplier used for making the liners (a high viscosity grade compatible with extrusion/injection). These different grades had slightly varying melting and degradation temperatures, resulting in a very narrow common temperature range of only 20°C, as shown in figure 12 below.

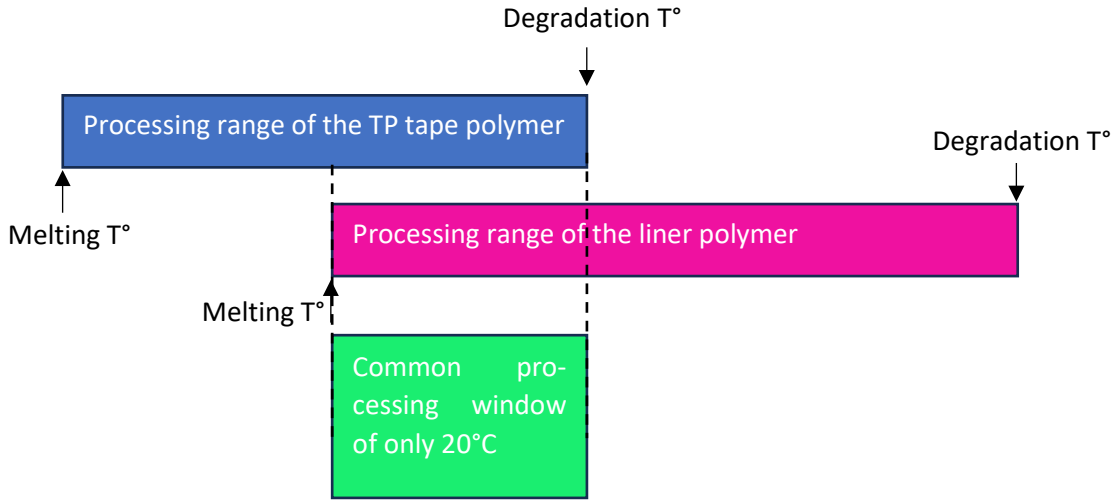

Figure 12: Narrow process window resulting from the different processing temperature of polymer A grade used in the TP tape and polymer A grade used for the liner

Additionally, the quality of the TP tape was low (with inconsistent width, thickness, and fibre distribution, as well as issues like self-slitting, fuzz, and broken fibres), making it very difficult to process and achieve high-quality composite material. Several prototypes made with Polymer A were tested using a pressure test setup specifically created for this purpose (WP5.2) shown in figure 13.

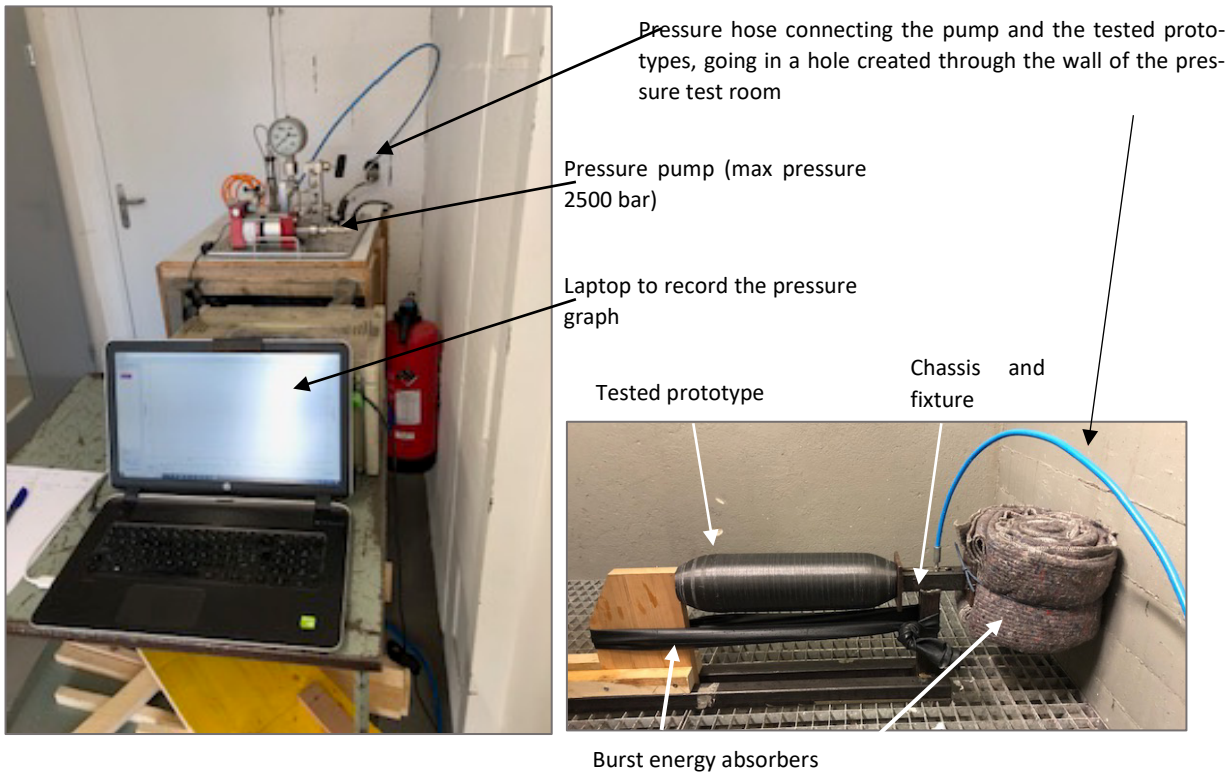

Figure 13: Pressure test setup

This pressure test setup was used to test dozens of liners up to 30 bars and more than 20 full composite prototypes up to over 1000 bars. It was modified and upgraded throughout the project.

Figure 14 below shows a liner during a burst test, figure 15 a full pressure tank prototype after a burst, and figure 16 is an example of a pressure test graph

Figure 14: Burst test of a liner

Figure 15: Pressure tank prototype after burst

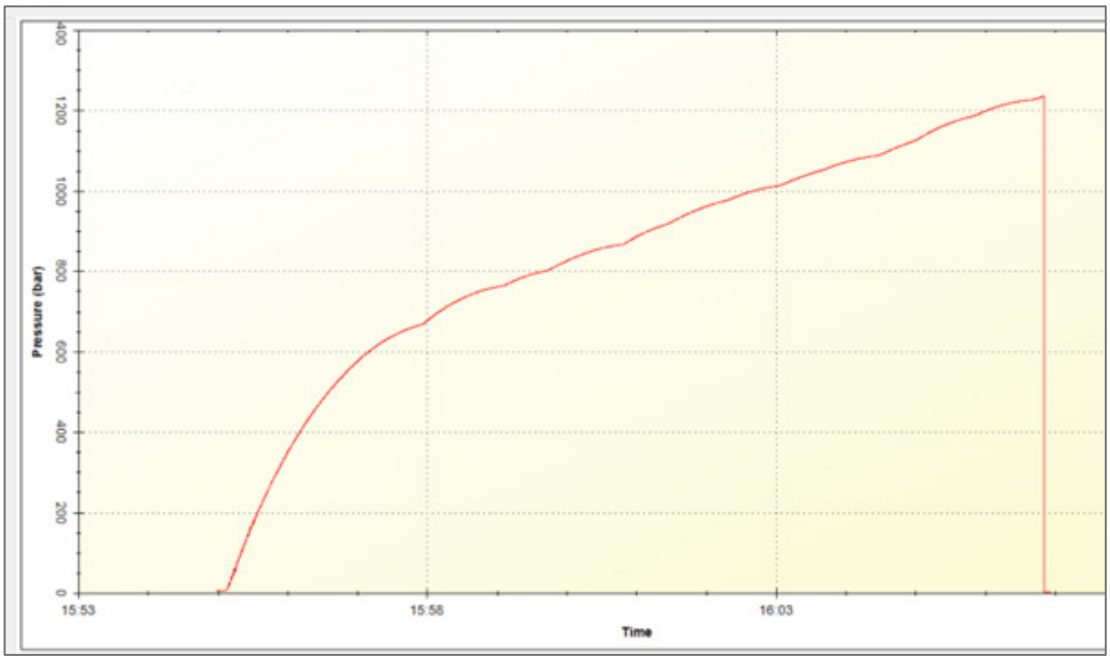

Figure 16: Example a graph showing the pressure measured in a tank prototype to burst

In parallel with the design–manufacturing–testing work and within the framework of Work Package 3, several material characterization tests were conducted, in addition to the tensile tests mentioned above, to support the overall development and provide the design and simulation model with material properties. A Nol ring test was developed to measure the tensile strength of a section of reinforced tube or pressure tank as shown on figure 17 below:

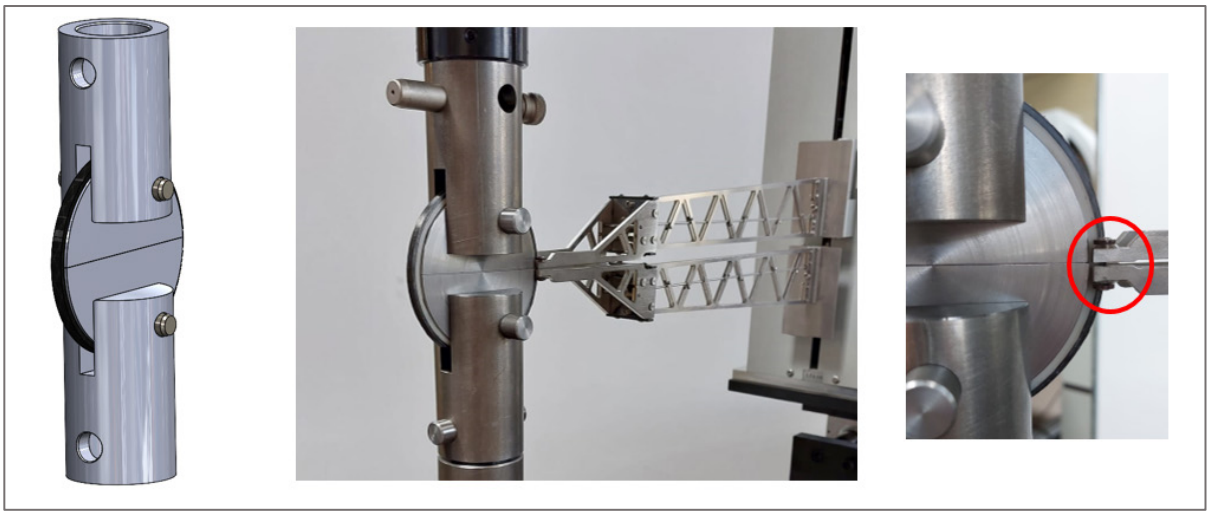

Figure 17: Nol ring test setup developed to evaluate the tank composite structure resistance

A fracture toughness test was developed as well to measure the load necessary to propagate a crack in a composite laminate (figure 18):

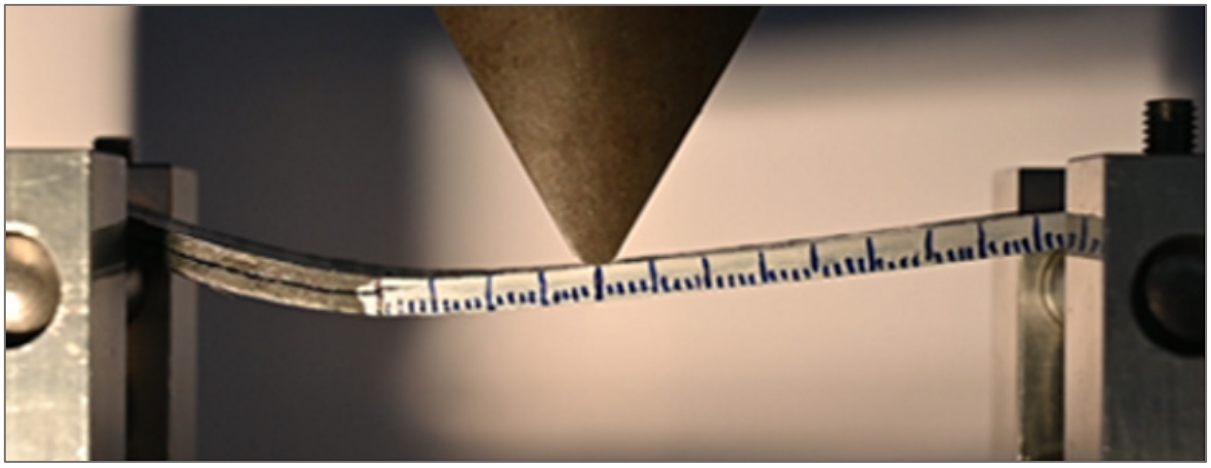

Figure 18: Composite specimen under fracture toughness test

In this test, a specimen with an intentionally created crack is subjected to a 3-point bending test, while a camera records the crack front position relative to the applied bending load. The results of this test were crucial for extrapolating the impact of potential manufacturing defects on the pressure tank structure, particularly in the end areas. The test was performed on several different composite materials.

Inter-Laminar Shear Strength (ILSS) measurements were performed on composite unidirectional and bi-axial laminates (figure 19). The results of these tests were used to refine the FEA model, adjusting the pressure tank geometry and the composite layers' thickness to meet the targeted performance of the tanks.

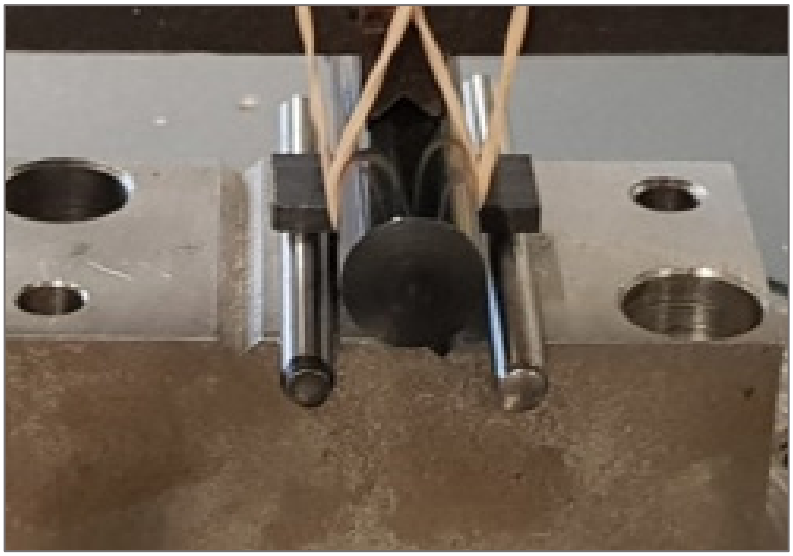

Figure 19: Composite specimen under ILSS test

The test results also highlighted a laminate manufacturing parameter that is particularly critical to the final quality of the laminate.

A peel test was developed from scratch to characterize the adhesion quality of prepreg tapes to liners and to adjust the process parameters accordingly. This test is presented in figure 20.

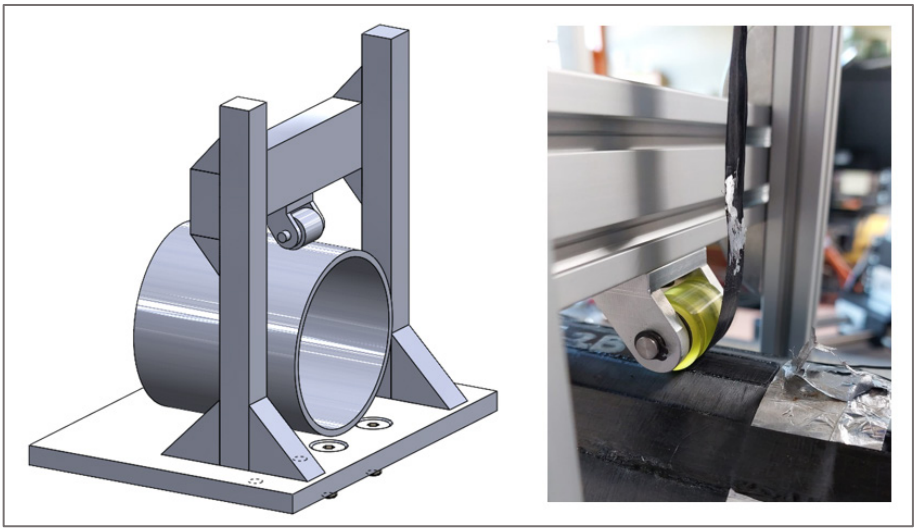

Figure 20: Peel test setup from conception (left) to implementation

For this test, a fixture was created to hold a tubular section of the liner and pull a piece of tape laid onto the liner section by Automated Fiber Placement (AFP) with in-situ consolidation. The test results allowed for the correlation of tape-liner adhesion quality with the process parameters.

The huge quantity of test results is presented in Appendix A.

WP6 – Recyclability Assessment – developed a method for recycling pressure tanks made from carbon fibres and two different polymers. This method can also be applied to recycle pressure tanks made from other thermoplastic composite materials. It involves cutting the pressure tanks into pieces, shredding these pieces, compounding the chips, and then injecting the compound into any mouldable component. The recycling process steps are shown in figure 21 below.

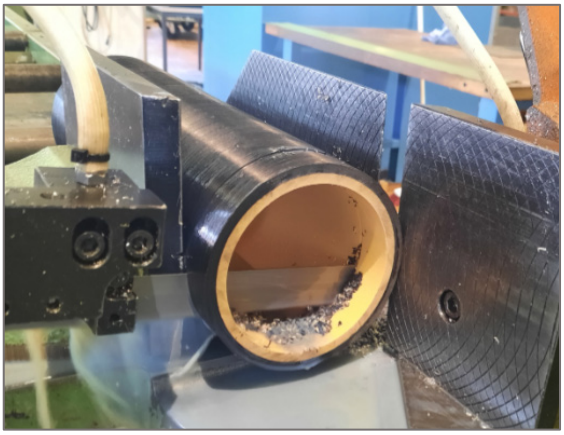

Pressure tank cutting

Shreding of the cut pieces

Chips obtained after shreding

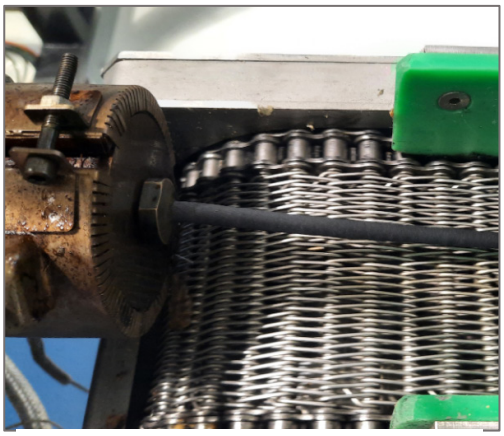

Compounding of the chips to get a consistent material

Injection of the compound into any injectable component, here tensile test specimen

Figure 21: Pressure tanks recycling process steps

The mechanical properties of the recycled material have been measured and found to be comparable with those of the original non-recycled material available on the market.

4 Work performed and results

The methods and experimental setups presented above have been used to develop a pressure tank geometry and manufacturing process that meets the targeted burst pressure level. A total of three design-manufacturing-testing loops were necessary. The table below summarizes the work performed, the challenges faced, the lessons learned, and the conclusions drawn:

	Work performed	
Loop 1 From 08-2022 to 07-2023	Simulation of several end-part geometries. Injection simulation on the selected geometry. Design and manufacturing of the injection mould and metal inserts while Carbon Fibre / PP prototypes were made based on the proof-of-concept design. Injection of liners' components with polymer A. Complete modification of the AFP machine. Processing trials of prepreg tape with Polymer A. Development of the welding method and process for liners assembly. Welding lines and liners testing. Manufacturing and pressure testing of tank prototypes.	Challenges Polymer A was very difficult to inject (high shrinkage creating cracks) and weld. Prepreg tape with Polymer A was of low quality and very difficult to process. The liner and prepreg tape joint process window is very narrow.
		Conclusion / learnings Polymer A was theoretically the best candidate, but its processability made it impractical for pressure tank manufacturing with the available equipment.
Loop 2 From 08-2023 to 01-2024	Modification of the end-part geometry and liner thickness. Modification of the injection mould accordingly. Injection of liners' components with 6 new polymer grades. Welding trials and liners assembly with the new materials Testing and processing of 3 new prepreg tapes Manufacturing and pressure testing of tank prototypes. Recycling trials with CF-PP based composite	Challenges Learn how to process the new materials (liner injection and welding + prepreg tape deposition) & characterize them all.
		Conclusion / learnings Easier material processability leads to better final product quality. Good liner polymer candidate & good prepreg tape candidate identified but compatibility between both materials not ideal. Specifications of the ideal materials clearly defined
Loop 3 From 02-2024 to 07-2024	Modification of the end-part and metal insert geometry. Modification of the injection mould accordingly. Injection of liners' components with 4 polymer grades (including 3 new grades). Welding trials and liners assembly with the new polymers and with the reference polymer. Testing and processing of 2 new prepreg tapes. Manufacturing and pressure testing of tank prototypes. Recycling trials with CF-Polymer A base composite	Challenges Learn how to process the new materials & characterize them. Achieve results consistency from one prototype to the next
		Conclusion / learnings Pressure tank design, material and manufacturing process parameters are strongly inter-related. We can reach the objectives with more than one material set (liner + composite) and for more than one application.

Table 1: Summary of the work performed through the 3 design-manufacturing-testing loops

During the first six months of the project, six pressure tank prototypes made of carbon fibres and PP polymer with dimensions close to the pilot customer's requirements were manufactured and tested, reaching a burst pressure of 613 bar (initial target was 800 bar). The liner end-parts of these prototypes were machined from a PP rod and assembled using hot plate welding with a tubular section of PP extruded pipe available on the market, close to the targeted diameter. Although PP was not suitable for the targeted applications due to its limited thermal resistance, it allowed the team to learn how to make prototypes and identify challenges. This work was carried out while WP1 and WP2 were being executed to design and manufacture the liner made of Polymer A, matching the pilot customer's exact specifications in terms of maximum length and diameter (to fit into the fuel cell bicycle frame).

Once liner components injected with Polymer A were available, extensive work was undertaken to learn how to assemble the liners by spin welding, test the quality of the weld lines, process the prepreg tape with Polymer A, and drastically modify and upgrade the Automated Fibre Placement prototype machine. Several pressure tank prototypes made of Polymer A were manufactured and tested, reaching a burst pressure of 543 bar. The processing of Polymer A to make liners and Carbon fibre–Polymer A composites turned out to be very challenging and incompatible with the reliable manufacturing of pressure tanks using the equipment and machines available for the project.

Loop 2 was then launched to modify the metal insert and liner geometry, adjust the mold accordingly, and make liners with six new polymers and full prototypes with three new prepreg tapes. Six tank prototypes were manufactured and tested, reaching 791 bar. In parallel, the analysis of standards (WP5.1) revealed that the safety factor should be raised from 2.25 to 3 to meet the requirements for the targeted application, which increased the minimum burst pressure target from 800 to 1050 bar.

During Loop 3, six full prototypes were manufactured based on the latest design version and tested, reaching a burst pressure of 1235 bar. Two material sets (liner polymer and composite polymer) were used successfully, and the ideal materials' performance and processability were defined.

In total, eight polymer grades have been tested for the liner, six prepreg tapes for the composite structure, tens of tank design variations have been simulated, three versions of the liner, metal insert, and injection mould have been designed and manufactured, tens of mechanical tests have been performed, and the recyclability of two composite material and liner sets have been assessed and proven.

5 Discussion

In the first loop of design, manufacturing, and testing of pressure tank prototypes, it was pointed out that the process window of Polymer A, the most promising polymer candidate identified during the POSSHYS project, was very narrow and incompatible with the initial tank design version and the available prototyping machine. The high rigidity (and consequently low elongation at break) and high shrinkage of Polymer A caused cracks to occur in the injected liner end-part around the metal inserts. Additionally, the quality of the carbon fibre–Polymer A prepreg tape was found to be low and critical for the final tank composite structure performance. More generally, as other prepreg tapes were tested, it was observed that the processing methods and parameters also significantly influenced the final composite material's mechanical properties. The graph below (figure 22) shows the shear resistance (Inter-Laminar Shear Strength) of two carbon fibre prepreg tapes, including tape with Polymer A, processed under ideal conditions (lab-scale laminates consolidated by autoclave) and processed by hot press and by Automated Fibre Placement with in-situ consolidation using NGT’s prototype machine.

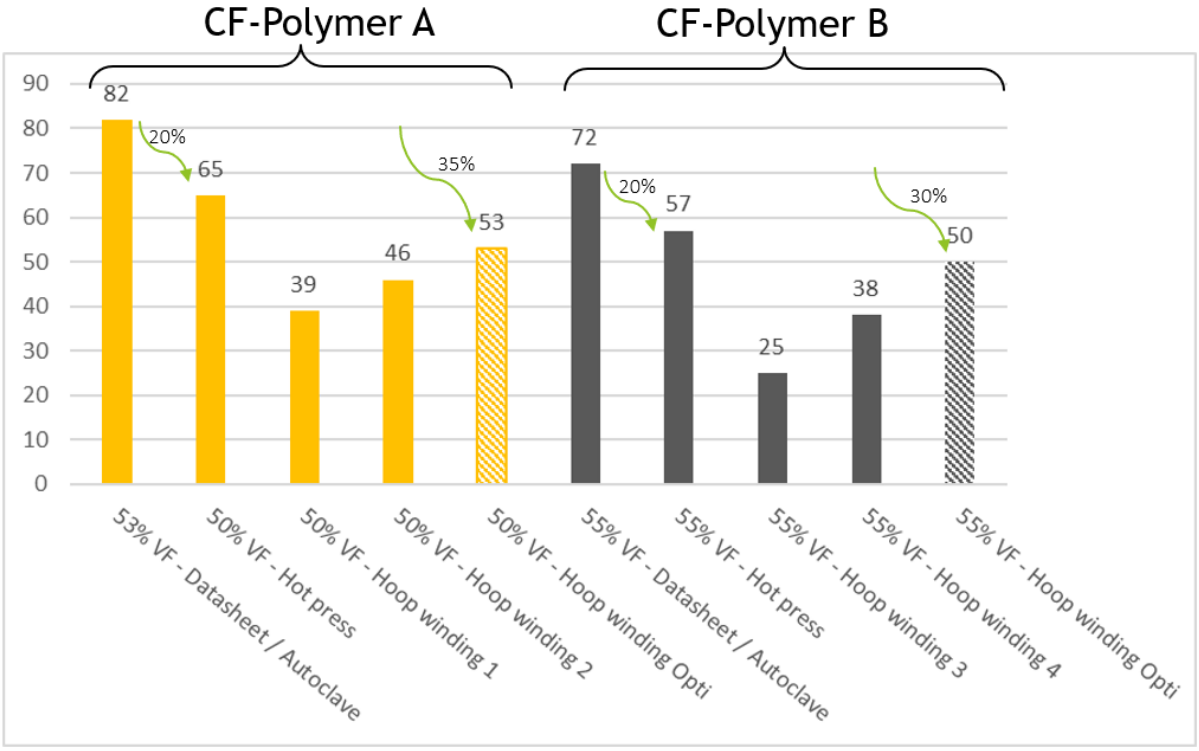

Figure 22: Drop in the composite material performance from a lab-scale laminate processed in ideal condition to the composite part material processed by AFP

The shear strength of the composite laminate made by hot press drops by about 20% compared to the level of the lab-scale ideally consolidated laminate. It drops by more than 50% when the laminate is made by Automated Fibre Placement (AFP) with in-situ consolidation. In-depth work to optimize AFP parameters allowed for some recovery of the material's performance potential, but the properties obtained through the industrial process generally remained 30 to 40% lower than those of the lab-scale ideally processed material. These observations on the performance drop, the tendency for cracks around the liner's metal insert, and the narrow process window of Polymer A led the project partners to reconsider the polymer selection criteria and focus further on polymer processability.

Design–manufacturing–testing Loop 2 was performed to test polymers and composites with a larger AFP and injection process window applied to a modified design. Specifically, the liner's wall thickness was increased to make the welding assembly easier and more reliable. The technical work performed during Loop 2, in conjunction with the analysis of relevant standards for the targeted applications, allowed for the identification of several liner-composite material sets compatible with the available manufacturing equipment, onboard hydrogen storage for fuel cell vehicles, and the transport of compressed hydrogen.

Design–manufacturing–testing Loop 3 further adjusted the liner design, especially in the metal insert region, as well as the composite structure design and processing parameters, to achieve the tanks' burst pressure levels specified in the relevant standards.

6 Further steps

Now that the material specifications relevant to the targeted hydrogen storage and transport applications, as well as to NGT's pressure tank technology - including processability -have been identified and successfully experimentally validated, further work is needed to optimize the performance of the pressure tank prototypes and conduct additional tests beyond burst pressure. More precisely, tests specified in standards ISO 11119-3, EN 12245, Regulation R134, and EN 17339 - relevant to fuel cell bicycle applications, fuel cell drones, road vehicles, and hydrogen transport, include pressure cycling, testing at -40°C and 85°C, impact resistance, damage resistance, etc. Many of these tests require specific equipment and expertise not available within the HYTMOB project partners. NGT will need to have these tests performed by external laboratories or in partnership with customers and other industry players.

Further improvement work on pressure tank prototypes will be necessary, based on all the test results and the tools and methods developed within the framework of HYTMOB. For example, the design and finite element simulation model will continue to be used to optimize the composite structure. The injection mould may be modified and used for additional liner component injection campaigns, for example to integrate the design of the welding profiles. The design and manufacturing of a production mould should also be considered based on the injection mould developed during HYTMOB. The experience and know-how gained from the welding assembly of the liner's components should be transferred to industrial welding machinery and process. NGT has already initiated work on TRL6, "Full-Scale Prototype / Field Demonstration," for the hydrogen bicycle application.

7 Conclusions

Although the project partners encountered unexpected difficulties, primarily related to the challenges of processing the initially selected material, HYTMOB has been extremely successful and has allowed us to reach and surpass the objectives. Not only has the pressure tank burst pressure target been achieved - despite being raised by more than 30% during the project - but also multiple material sets have been identified and tested to meet the technical specifications of several possible applications. The excellent collaboration between the project partners has enabled the development of the tools, methods, know-how, and expertise necessary for the project's success and future projects in the field of compressed gas storage and transport.

The pressure tank technology supported by HYTMOB advanced from early TRL4 to fully validated TRL5. These positive results have allowed the industrial project partner to attract new prospects and initiate discussions for further projects and potential applications. The project partners would like to warmly thank the Swiss Federal Office of Energy for its continuous support

8 Outlook and future implementation

The short-term focus of NGT remains the development of a small-dimension pressure tank for storing compressed hydrogen in a fuel cell bicycle. This work will be completed with pressure tank optimization, testing, and certification according to the relevant standards (ISO11119-3 [1] and/or EN12245 [2]). This certification, although complex and expensive, is one of the most achievable among hydrogen pressure tank certifications and could be validated by late 2026. It involves passing all the tests described in the standards and demonstrating the company's ability to perfectly control its manufacturing process and reproduce the performance of the tanks tested during the certification procedure. Therefore, a quality system must be built and implemented.

Once NGT has its first pressure tank model certified, it will focus on manufacturing and selling the certified model for hydrogen bicycles and drones. In parallel with the current small-dimension tank development, and thanks to the positive results of HYTMOB, NGT has initiated discussions with industrial players in the fuel cell road vehicles and hydrogen transport and distribution market segments. These players are seeking solutions that surpass state-of-the-art options, which include pressure tank recyclability (addressed by the thermoplastic nature of liners and composites tested during HYTMOB), conformability, and efficiency (addressed by NGT's concept and tank designs advanced during HYTMOB), as well as other application-specific features.

It is highly likely that at least one collaboration will begin in the near future regarding the development of a hydrogen tank for an industrial application, to be commercialized by 2029-2030.

9 National and international cooperation

The HYTMOB project was extremely successful in building a strong and efficient collaboration among the project partners. While NGT, as the project holder and industrial partner, faced a significant hardware product development challenge, the complementary contributions from HEIG-VD Comatec and HEIA-FR iRAP were essential in achieving the objectives. Further collaboration among the partners can be expected.

During the project, relationships with international industry players were established. Materials suppliers such as Arkema, BASF, Syensqo, Evonik, Sabic, and others have shown keen interest in proposing polymers for evaluation in the development and manufacturing of thermoplastic composite pressure tanks. These players have identified the hydrogen storage and transport market segment as a strategic business opportunity for the coming decades and are seeking the right technology to position their products. NGT is likely to strengthen its relationship with some of these polymer suppliers in the future. Thanks to the know-how, expertise, and understanding of hydrogen storage challenges that Comatec and iRAP have built and deepened during the project, they may also be part of future project consortiums.

Last but not least, the positive outcomes of the project have allowed NGT to further de-risk its technology development, gain credibility, and engage with new prospects in the field of hydrogen transport and distribution, as well as fuel cell vehicle manufacturing for road applications, light aviation, and drones. There are opportunities for cooperation and possibly joint development with some of these European prospects in the near future.

10 Publications

An article written by the project partners has been published in the international JEC Composites Magazine, issue N°152, entitled "A new paradigm for hydrogen pressure tanks":https://digital-magazine.jec-composites.com/jec-composites-magazine/jec-composites-magazine/n152-2023

NGT has been invited to present at the worldwide symposium about composite pressure vessels COPV World 2023 Belgium (Hasselt) in December 2023 were 100 international experts in pressure vessels had the opportunity to share, discuss and network: https://www.linkedin.com/posts/axel-seifert-0a720126_copv-world-2023-agenda-activity-7125104933820862466-b4UX/

11 References

[1] ISO 11119-3:2020 Gas cylinders — Design, construction and testing of refillable composite gas cylinders and tubesPart 3: Fully wrapped fibre reinforced composite gas cylinders and tubes up to 450 l with non-load-sharing metallic or non-metallic liners or without liners

[2] EN 12245: 2022 Transportable gas cylinders - Fully wrapped composite cylinders

[3] EN 17339: 2020 Transportable gas cylinders - Fully wrapped carbon composite cylinders and tubes for hydrogen

[4] R134: Regulation No 134 of the Economic Commission for Europe of the United Nations (UN/ECE) — Uniform provisions concerning the approval of motor vehicles and their components with regard to the safety-related performance of hydrogen-fuelled vehicles (HFCV) [2019/795]

12 Appendix

Appendix A: Work package 1 “Pressure tank design and simulation” and work package 3 “Materials characterization” detailed report

Appendix A: Work package 1 “Pressure tank design and simulation” and work package 3 “Materials characterization” detailed report

July 2024

Authors:

Raphaël Nardin, Mehdi Meguenni, Prof. Joël Cugnoni

Table of contents

1 Introduction

This report describes the work that was done by HEIG-VD (School of Engineering and Management Vaud) during the HYTMOB project, which was supported by SFOE (Swiss Federal Office of Energy) and in partnership with NGT (New Generation Tanks) and the iRAP institute (Institute for Applied Plastics Research).

Most type IV hydrogen tanks are made of composite materials including a thermoset matrix (epoxy), and produced using a filament winding process involving two main drawbacks: tanks are limited to a small range of aspect ratio (length/diameter) and most carbon fibers are not used to their full potential because they are not necessarily aligned with the main stress directions.

NGT's technology enables extending the tanks aspect ratio to a wider range and placing fibers in the optimal directions: longitudinal (0°) and circumferential (90°). Therefore, tanks are lighter and easier to integrate to vehicles. Moreover, the use of thermoplastic materials makes them recyclable, unlike current type IV hydrogen tanks.

After the POSSHYS project (Polymer Screening for Hydrogen Storage), polymers were evaluated and selected for NGT's tanks technology in industrial applications. In this project, the goal is to develop a hydrogen tank prototype, which could be used by a potential client in the context of hydrogen bikes. The project was divided in work packages and this report summarizes the tasks of the work packages achieved by HEIG-VD:

- WP1: tank simulation and design
- WP3: materials characterization

2 WP1: tank simulation and design

2.1 Initial design specifications

The tank design concept is described in Figure 1. It consists of aluminum inserts embedded into a thermoplastic liner, on which the thermoplastic composite tape is placed. There is one "entry" insert and one "bottom" insert. They form the tips of the tank and allow connecting it to other devices like valves and pressure relief devices. The liner is divided in several parts: the bases, at the tips, are over-molded on the inserts before being welded to the other tubular parts. It ensures gas tightness and acts as a mandrel for fiber deposition. Finally, the thermoplastic composite tape is meant to be placed either along the tank main axis (0°), or in the circumferential direction (90°). The fibers are the structural component which resists the internal pressure. Initially, NGT's concept places 0° layers on the liner, on top of which 90° layers are wound.

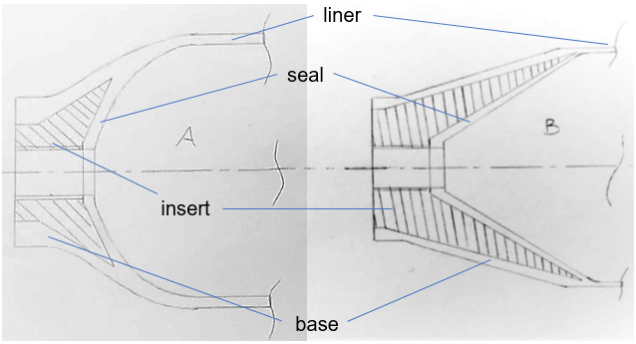

Figure 1: sketch of NGT's tank concept

Below are listed more technical design specifications for the first tank prototype. More specific requirements, such as failure criteria, will be introduced later.

Table 1: design specifications

Service pressure	350 bar
Safety factor	2.25 for burst initially and then 3
Maximum dimensions	D=116mm, L=427.5mm
Hydrogen volume	~3L, to maximize
Internal shape	“Convex” (liquid must not be trapped inside)
Cone angle	To minimize for process / to maximize increased storage volume
Mass	To minimize
Insert material	Aluminum 6061
Insert threading	M18x20mm (ISO15245-1)
Liner material	Polymer A, B, C, D
Liner thickness	2-3mm (initial)
Composite tape	Polymer A-CF, Polymer B-CF, 10 to 12mm UD tape
Composite layup angles	0°, 90°
Max length for molding	110mm (iRAP injection press stroke)

2.2 First design: Polymer A-CF

Composite thickness

At first, the tank can be divided in three parts: the cylindrical part, the transition part and the tip. In each part, one can expect issues which may differ. For example, it is already known that interlaminar shear is high in the transition region. Here, composite thickness is firstly designed regarding the cylindrical part, since in that part the diameter is the largest and the composite layers are the thinnest. Indeed, 0° layers overlap each other outside of the cylindrical part, and 90° layers as well, especially in the conical part (Figure 2).

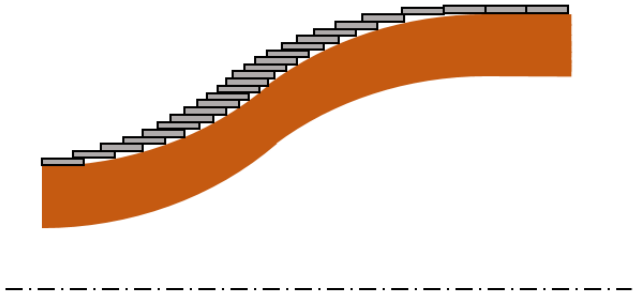

Figure 2: 90° UD tape winding

In the cylindrical region, the principal stress directions are axial and circumferential, hence along the fibres. A maximum deformation failure criterion is used and the thickness approximations can even be found analytically. With the burst pressure $p = 2.25 \cdot 350 = 787.5$ bar, the diameter $D = 116$ mm, the allowed deformation $\varepsilon = 1.3\%$ and the composite longitudinal elastic modulus $E_1 = 140$ GPa, it yields

$$t_0 = \frac{pD}{4\varepsilon E_1} = 1.25 \text{ mm}, \quad t_{90} = 2t_0 = 2.5 \text{ mm}.$$

The deformation value comes from measurements (see 4.2 Traction (composite)): delamination starts occurring at 1.3%. It is safer to use this value than the value for failure (~2%). The formulas above are valid under the assumption that the thickness-to-diameter ratio tends to zero, that the liner has zero stiffness and that the lateral stiffness of the composite is ignored as well.

To get more accurate results, the thicknesses obtained above can be inserted in the finite element (FE) model and tuned iteratively until the axial and circumferential deformations reach 1.3% in the cylindrical part. The other relevant parameters are shown in the table below. The obtained thicknesses are $t_0 = 0.9$ mm and $t_{90} = 2.26$ mm and it was verified that fibres deformation does not exceed 1.3% at any location of the tank. From these results, the liner external diameter was set to 106.5 mm to ensure the 116 mm specification would not be exceeded and because NGT was using tubes of this size.

Table 2: mechanical properties of the composite and the liner

Parameter	Value	Comment
Composite E1	140 GPa	T700 fiber at 60% volume fraction ; confirmed by tests
Composite E2	6500 GPa	T700 fiber at 60% volume fraction (mixing rule)
Liner E	2.5 GPa	Polymer A data sheet
Liner ν	0.4	Common value for thermoplastics
Liner thickness	2.5 mm	From specifications

Cone angle optimization

At the endpoint of the tank, the diameter must somehow be reduced to close it. The tip of the liner must remain “horizontal”, *i.e.* end up being parallel to the tank main axis to allow starting the 90° tape winding on a regular cylinder portion. So, the diameter is assumed to vary smoothly from the small to the large diameter, following a sinusoidal curve. The cone angle is related to the transition length and to the diameters. A more open cone angle prevents the inserts from being pushed out of the tank, but

it increases interlaminar shear in the 0° composite layer. Moreover, from a processing point of view, it is difficult to wind 90° tape when the cone becomes too open (above ~30°-35°).

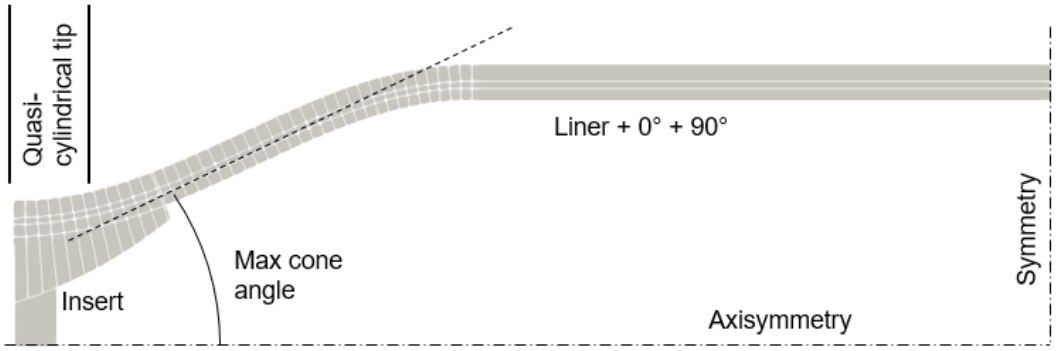

Figure 3: geometry generated by the parametric FE model

Figure 3 shows the geometry generated by the parametric FE model for a maximum cone angle of 25° and a small diameter of one half of the large diameter and assuming constant composite thicknesses. At this stage of the project, the model was axisymmetric (2D), static, linear, and treated all contacts as perfectly bonded. The seal was not modelled yet and the insert geometry was rather simple (generated automatically as well) to allow simulating multiple cases quickly.

As explained previously, a crucial mechanical aspect of the transition region is the interlaminar shear in the 0° layers. Figure 4 shows that the largest peak is located at the boundary of that region with the cylindrical part. It is due to the bending moment resulting from the axial component of the pressure pushing against the end of the tank. There is a lower peak at the inflection point, and other high values in the insert zone, which is treated separately in detail later. Composite laminates made of the Polymer A-CF tape used here have an interlaminar shear strength (ILSS) of 67 MPa (cf. project POSSHYS). However, the measured in-situ ILSS did not exceed 40MPa (see 4.6 Interlaminar Shear Strength (ILSS)). So in this configuration, any cone angle below 35° should be fine regarding this failure mode. Considering NGT's feedback on processing aspects, there was an agreement to choose a cone angle lower than 35°.

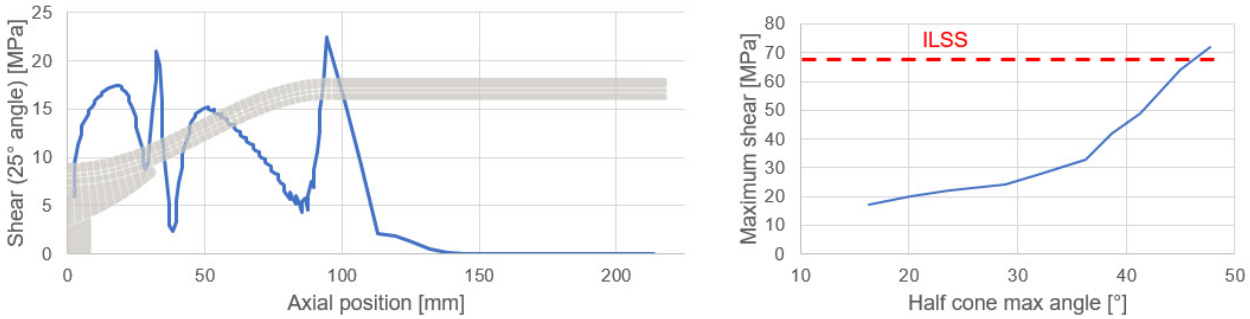

Figure 4: interlaminar shear in the 0° layer

First design adjustments

A few points evolved to meet processing requirements or to optimize the tank (see Figure 5):

- The slope in the design described in Figure 3 is longer: more suitable for processing.
- The radius of 37.5mm in the transition zone was optimized to maximize hydrogen capacity while not making interlaminar shear exceed the ILSS.
- A seal with grooves was included.
- Grooves were added to the external face of the insert to prevent rotations between the liner and the insert when screwing connecting devices.
- The liner tip diameter was optimized: for a given insert length, a larger diameter implies a larger projected surface, hence a larger axial force against the liner.

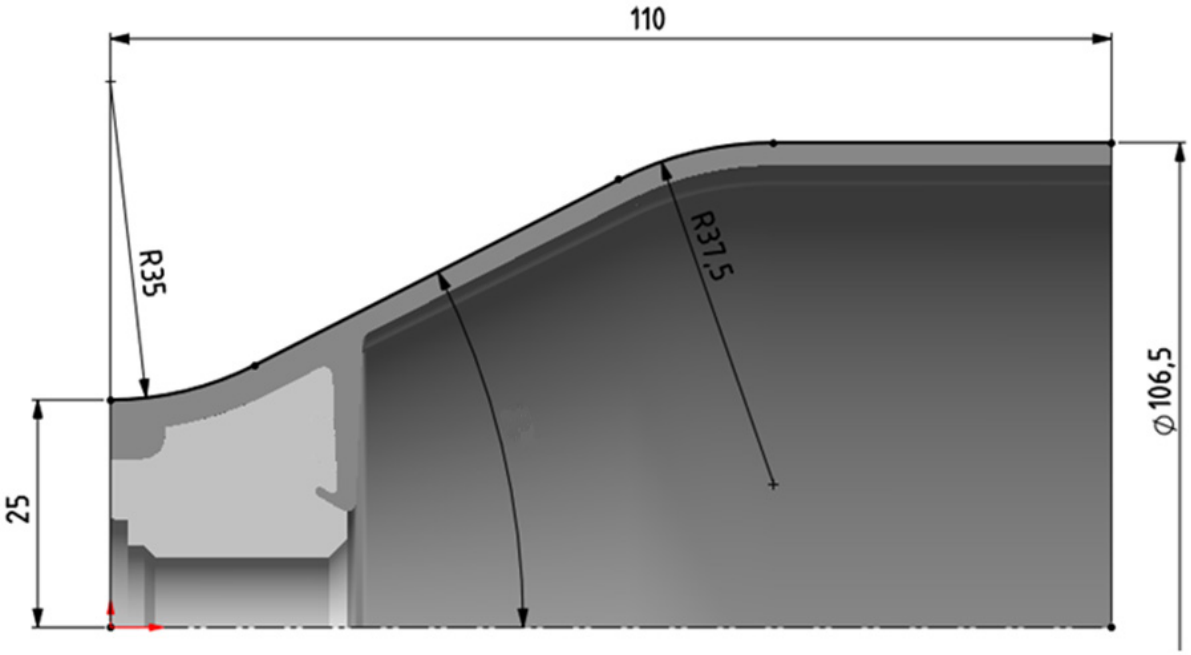

Figure 5: design modifications

For this last point, two cases were simulated: the first one with a bonded contact between the insert and the liner, and the second one with a sliding contact. Reality stands somewhere in between. In both cases, looking at the Von Mises equivalent stress in the liner (Figure 6), there is a large peak at the insert-liner contact area. In this configuration, with most parameters already optimized, it is difficult to reduce these peaks given the large amount of pressure applied (burst pressure: 787.5 bar). However, it is important to keep in mind that:

1. At this stage, the model was still linear elastic, so stresses are overestimated for ductile materials. In reality, Polymer A plastifies and such local stress concentrations are actually redistributed.
2. The largest peak is located where the tip of the insert meets the liner. There is a numerical stress concentration, which does not exist in reality.
3. Here, a Von Mises failure criterion approach is used; but in this case, the liner is in such a highly compressed state that a Drucker-Prager criterion could be more suitable. This criterion implies

that materials undergoing a high hydrostatic stress state can resist higher deviatoric stresses. In other words, the red dashed line showing theoretical failure in Figure 6 is actually higher.

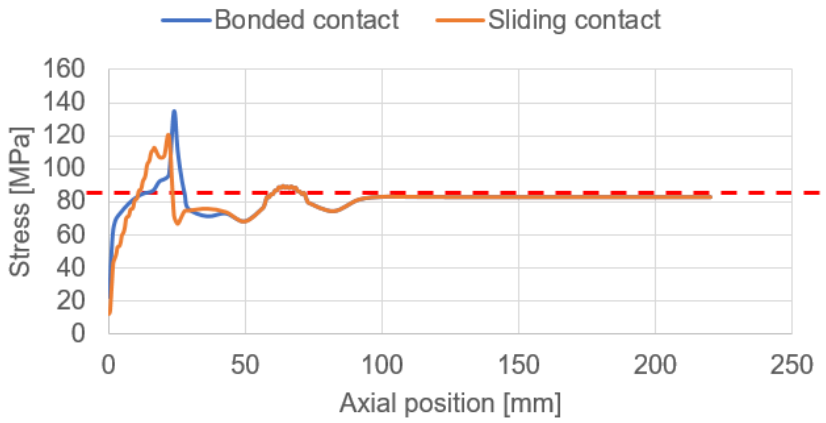

Figure 6: Von Mises equivalent stress in the liner

Crack propagation study

With this geometry, NGT's prototypes happened to burst at only 200 to 300 bar. At first, delamination occurs between the 0°/90° interface. Then, large cracks propagate in the 90° layer at the end of the cylindrical region and the whole cone made of 90° layers pops out (Figure 7). Although the composite may not reach its ILSS, defaults such as voids and cracks introduced during the process can still propagate and cause failure.

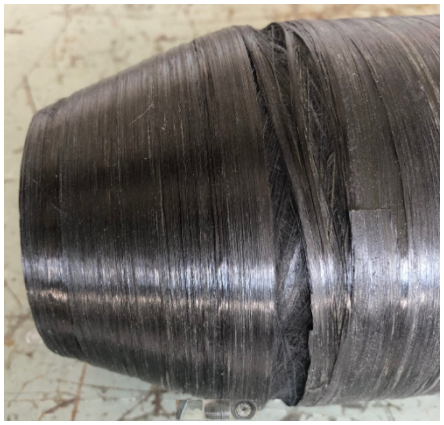

Figure 7: burst test of a Polymer A-CF tank prototype

To have a better understanding of the phenomenon, the linear FE model was improved to nonlinear cohesive, to model crack propagations at the 0°/90° interface. The new parameters to set are the ILSS of the composite and the mode II interface toughness G_{2c}.

A simulation of the current geometry was performed with an ILSS of 45 MPa and $G_{2c} = 800$ J/m^2 (see 4.5 and 4.6), and with a 5mm-long default located on the top of the cone (worst case scenario). It showed a crack initiation at 360 bar and an unstable crack propagation at 450 bar (Figure 8).

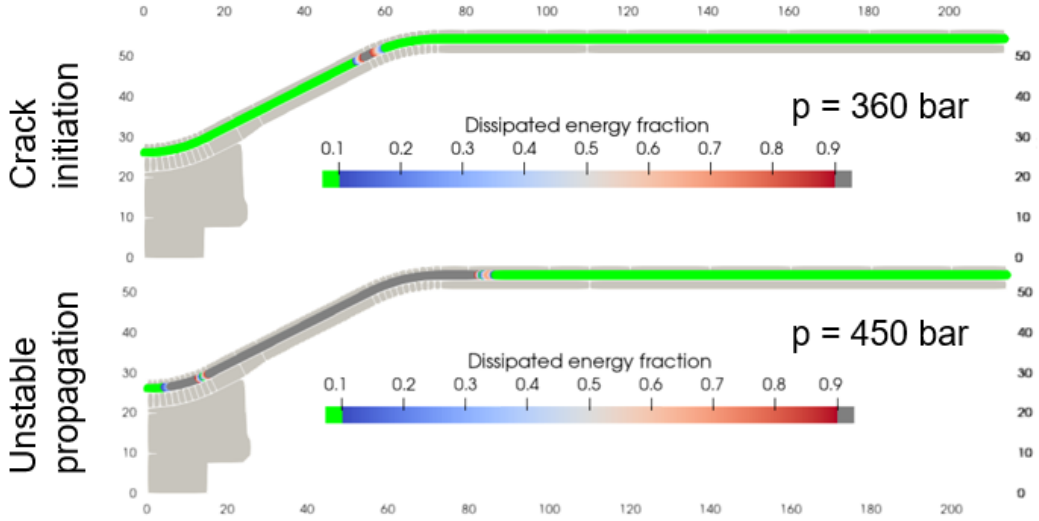

Figure 8: cohesive model simulation results

One solution to improve these issues is to have more 0°/90° layer alternations. A [0°, 90°, 0°, 90°] architecture can decrease interlaminar shear in the conical region. Based on that, four scenarios were simulated:

1. [0, 90] without default
2. [0, 90] with a 5mm-long default at the interface at the top of the cone
3. [0, 90, 0, 90] without default
4. [0, 90, 0, 90] with the same 5mm default at the first 0/90 interface

Note that the first 0° layer undergoes more shear than the second one, so cases with a default in other interfaces are not presented here. Each scenario was simulated with a best case (B) and a worst case (W) scenario of materials properties. The values come from measurements (see 4.4, 4.6).

B: best case ; $G_{2c} = 1200$ J/m^2, ILSS $= 65$ MPa, $E_1 = 140$ GPa

W: worst case ; $G_{2c} = 500$ J/m^2, ILSS $= 33$ MPa, $E_1 = 100$ GPa

Here are the main conclusions that can be drawn from the results, summarized in Figure 9:

- Crack propagations do not systematically occur at a larger pressure with 4 layers
- With 2 layers, crack propagations are always unstable, leading to sudden and dramatic failure
- Crack propagations are very stable with 4 layers (it is clear when visualizing results like they are presented in Figure 8)
- The quality of the materials and of the processing is more important than the architecture of layup
- Finally, the 37.5mm radius of the transition region (Figure 5) was increased; it turned out to delay the first crack propagation efficiently because it decreases interlaminar shear

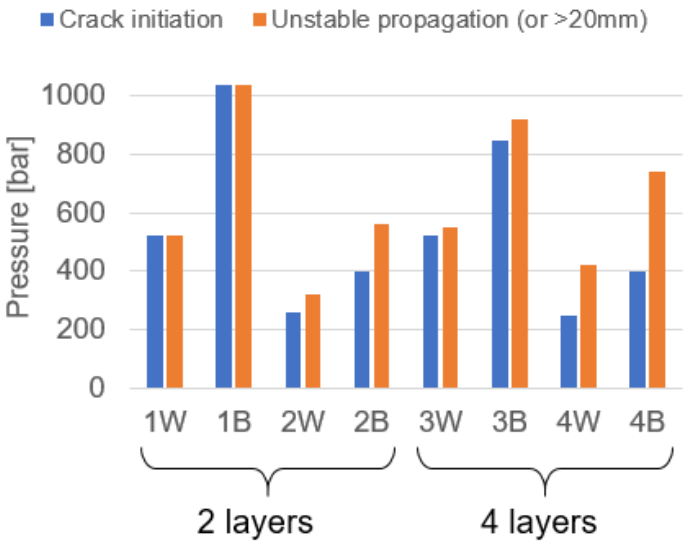

Figure 9: simulation results of the cohesive model for Polymer A-CF

Note that with NGT's process, layers are thicker at the tips of the tanks, which was not modelled in this study. Based on these results, it is clear that for the next prototypes, a [0, 90, 0, 90] layup will be used, and it is worth putting some efforts and time in improving the quality of the process.

Issues with Polymer A material

Despite the efforts put into improving the process quality and trying various techniques to make prototypes bear higher pressures, two major issues remain very difficult to deal with when working with Polymer A:

1. The processing window of Polymer A is narrow and even though the mechanical properties of hot-pressed plates can get close to the suppliers' datasheet properties, the in-situ properties are too poor. Indeed, the processed composite looks dry and its ILSS only reaches 33 MPa (see 4.6), which is not enough to sustain the shear that 0° layers undergo. Moreover, 0°/90° interfaces are particularly weak as well. This is why even with external steel reinforcements, Polymer A tank prototypes did not reach more than 550 bar (Figure 10).

Figure 10: burst test; the Polymer A-CF prototype burst at 550 bar

2. The Polymer A liner breaks very easily at the tip of the tank around the insert (Figure 11) because of Polymer A's rather large coefficient of thermal expansion (CTE): $7 \cdot 10^{-5}$ $C°^{-1}$ up to

100°C and more above, against $1.3 \cdot 10^{-5}$ $C°^{-1}$ for aluminum. When it cools down after being over-molded, it is subject to residual stresses due to the difference between the CTE of Polymer A and aluminum.

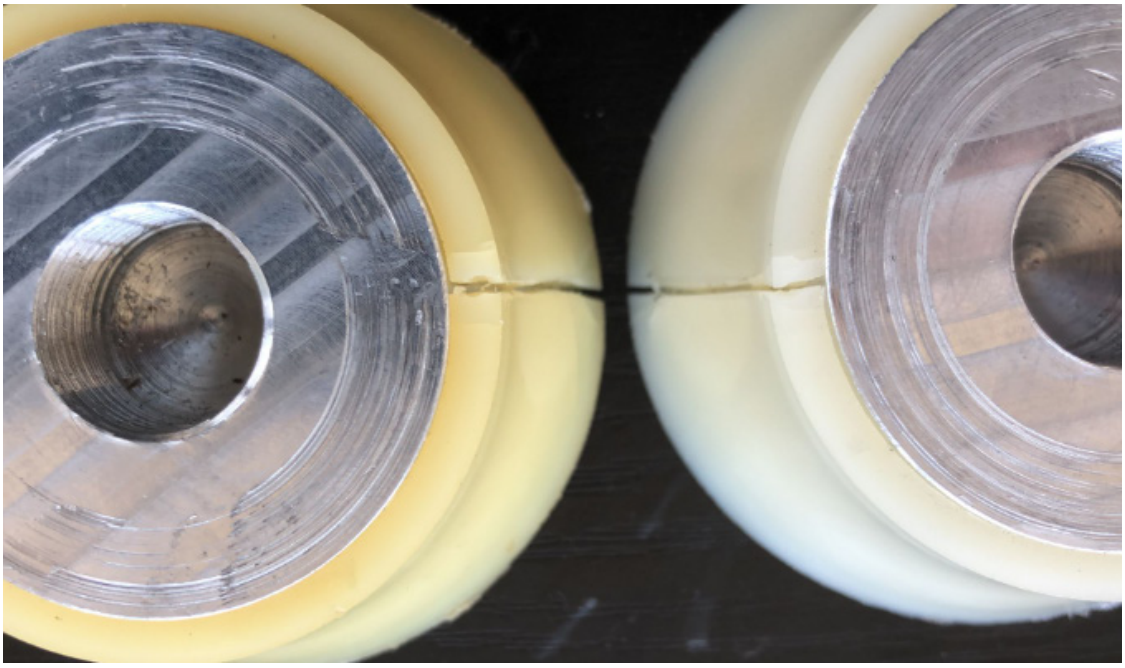

Figure 11: cracks in the liner at the extremity

Thermomechanical simulations show that after cooling, the Von Mises equivalent stress reaches 20 MPa at the base of the seal when we assume that deformations are frozen at 100°C. This scenario is similar to the relaxation treatment with slow cooling up to 90°C that is recommended by the supplier (BASF). With a quicker cooling, that freezes deformations at 150°C, residual stresses reach 40 MPa at the base of the seal. Since the tensile strength of Polymer A is about 85 MPa, these residual stresses are too high for the unpressurized state.

Annealing cycles were investigated, as well as heating the insert to higher temperatures, but finally, residual stresses just depend on the materials CTE and cannot be avoided.

Because of the issues detailed above, Polymer A was put aside and the design process continued with other materials.

2.3 Second design: Polymer B liner & Polymer F-CF composite

New materials selection

A few other semi-crystalline thermoplastics were considered to replace Polymer A, each of them having their pros and cons regarding price, processing temperature and mechanical properties.

- **Polymer B:** high deformation at break and low processing temperature, making it compatible with hot plate welding.
- **Polymer C:** high yield stress but low deformation at break, thus quite brittle. Although some characterization tests were promising, the 90° max deformation of the composite is expected to be low. Specially formulated grades are necessary to overcome this limitation.
- **Polymer D:** expensive and high processing temperature, but becoming a reference in aerospace applications. Could be a benchmark for NGT's technology.
- **Polymer E:** low processing temperature and high compressive yield stress, but low deformation at break.

Since Polymer B was a good candidate from different perspectives and material was in stock quickly, NGT decided to use it to make the next liner prototypes. The shrinkage issues encountered with Polymer A were solved. As for the composite, no prepreg tape with Polymer B as matrix was available, so NGT tested a Polymer F-carbon fiber tape with a processing temperature very close to Polymer B and high resin content, making its processing easier and the final quality visually much better. These materials were therefore used for the next prototypes.

Liner extrusion issues

With the first Polymer B (for the liner) / Polymer F-CF (for the structure) prototype, the burst test pressure reached 548 bar. A new issue appeared: the liner was actually extruded because of the high compression between the insert and the composite. This allowed the insert to slide outwards, pulling the seal with it and initiating a crack at its base (Figure 12).

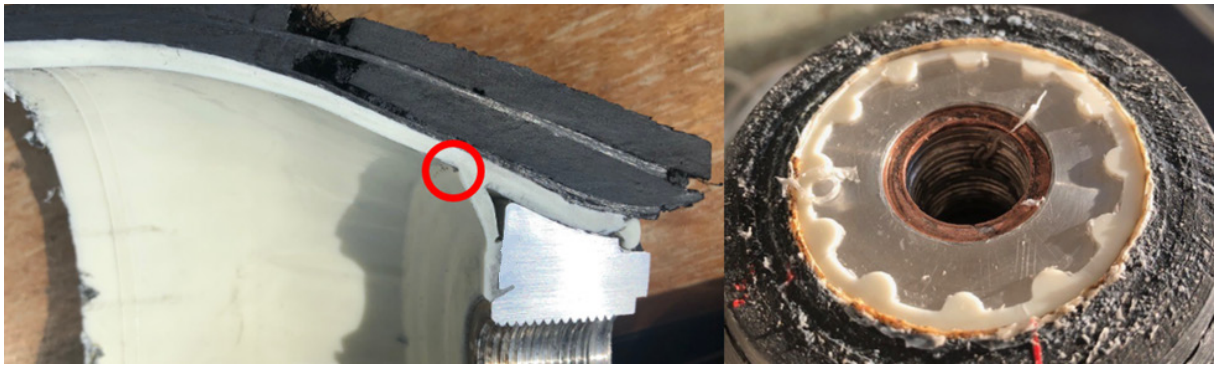

Figure 12: tank failure due to the extrusion of the liner

Polymer B has a lower yield stress indeed: 63 MPa against 85 MPa for Polymer A. To investigate and solve this problem, plasticity was implemented in the FE model with a linear strain hardening constitutive law. Polymer B's stress-strain compression curve was measured (see 4.4 Compression), and all liner interfaces from the tank tip to the cone end were modelled as sliding interfaces: the

liner/composite interface may break, allowing the liner to slide out of the composite. In simulations, both scenarios are generally studied: broken and intact interface.

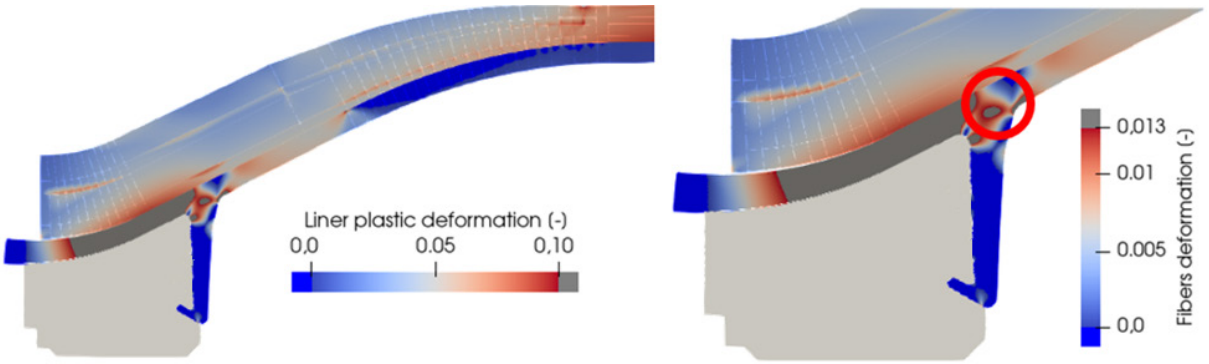

Figure 13: elastoplastic simulation of the 548 bar burst pressure test

Figure 13 shows the plastic deformations in the liner and the deformations along the carbon fibres with a 548 bar pressure. It confirms that the compression of the liner between the insert and the composite is too high: plastic deformations are above 10% and allow the insert to slide 1.22mm out of the composite, causing high stresses at the base of the seal. The simulation enables defining a failure criterion for the liner. As it is difficult to tell what exact stress or strain distribution breaks the liner, one can tell that if the insert displacement reaches about 1.2mm, the seal is likely to break. This criterion is valid for this seal design.

Design modification

To prevent the scenario explained above from happening, the liner portion between the insert and the composite must be removed, such that the liner is in direct contact with the first composite layer. The contact stiffness will be much larger, the insert will slide much less and the deformations in the seal will be smaller. Moreover, the fillet at the base of the liner is removed as well so the half cone angle is constant at a steady angle. The fillet allowed initiating the 90° layers more easily. Without it, the solution for NGT is to start depositing on a cylinder outside of the tank that is cut afterwards. This allows having a larger area of contact with the same angle, distributing the load from the insert to the composite more evenly. With this new design, the simulated insert displacement went from 2.5mm down to 0.5mm at 787 bar. Finally, the mould was modified accordingly.

This design can still be optimized to decrease the stress in the seal. What happens here is that the seal acts like a beam cantilevered at its base. If it is more aligned to the rest of the liner, the bending and shear efforts at its base will be converted to simple traction efforts and the remaining plastic deformation peak will vanish. It is illustrated in Figure 15. With this design, there is no stress concentration in the liner anymore, whether the liner stays stuck to the composite or not.

In the final design, metal insert has sealing grooves placed closer to the main axis of the tank to increase the seal length. Moreover, it has pins to prevent rotations of the insert relatively to the liner when handling it, as well as smooth grooves at the tip to lock rotations between the insert and the composite. Indeed, when screwing a cap or valve into the insert, it must withstand a torque of 100Nm without rotating, so the design of 24 grooves was optimized such that this torque induces at most only

10MPa of shear in the composite. Finally, some holes are drilled to allow using a pin wrench when screwing the cap of the tank.

2.4 Tank performances

The next tank prototype with Polymer B liner and Polymer F-CF composite showed a burst pressure of 791 bar. This design did not correspond to the last one because the updated inserts were not available yet, so it corresponds to a hybrid design (Figure 16) which features the older insert and the steady slope was machined to extend it up to the extremity. The failure occurred in the composite because of fiber break and interface delamination. This means that even with this suboptimal design, the tip of the tank is not the weak point anymore.

This exact test was simulated to evaluate the potential performances of NGT's tanks in terms of achievable dry fibre to hydrogen weight ratio (at service pressure). Here is a summary of the key results, detailed in Table 3:

- The achieved fibre to hydrogen weight ratio is 13.91 for this 427mm-long prototype.
- According to simulation, the highest fibre deformation is 1.13% (1st layer, transverse). If we assume that the process could be improved, such that fibres would break at 1.3% (see 4.3), the burst pressure would increase to 897 bar and the fibre to hydrogen ratio to 12.56.
- The ratio decreases with the tank length. The longer the tank, the closer the ratio is to the performances cylindrical part alone. If this prototype was "infinitely" long, the ratio would be 9.66.
- If this prototype was "infinitely" long, and that fibres broke at 1.3% of deformation (897 bar), the ratio would be 8.67.
- Lastly, it is interesting to see that in the cylindrical part, the highest fibre deformations reached 0.85% to 1.13% depending on the layer. According to the simulation, if for the same burst pressure, the thicknesses of 0° and 90° layers are optimized, the deformations of all layers can reach the deformation causing failure together, making the tank more optimized. This is achieved with 0° layer thicknesses of 0.63mm and 90° layer thicknesses of 1.67mm (Figure 17). With these dimensions, optimized such that all layers reach 1.3% of deformation at 791 bar, the best achievable ratio is 7.31.

Table 3: tanks fiber-to-hydrogen weight ratio

	Current performance	Fibers reach 1.3%	Fibers reach 1.8%
Proto 427mm	13.91	12.56	9.75
Proto 1m	11.25	10.16	7.89
Proto 2m	10.42	9.41	7.30
Proto "infinite"	9.66	8.71	6.75
Proto "infinite" optimized	-	7.31	4.99

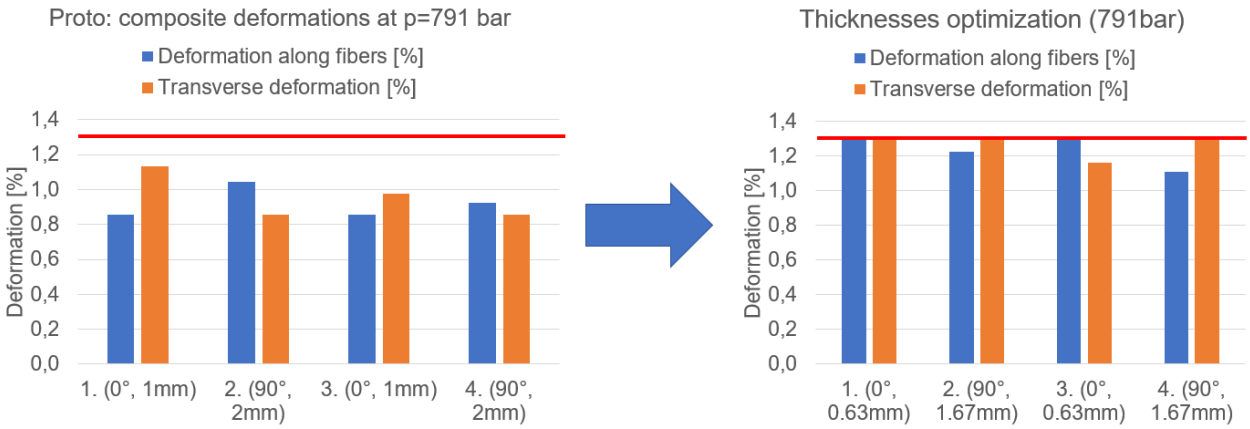

Figure 14: optimization of composite layers thickness

2.5 Improvement of Polymer F-CF design

New Geometry

After a set of tests, the tank's design has been optimized to achieve to the geometry bellow. This geometry has allowed, the avoidance of extrusion issues previously encountered by removing the portion of the liner between the insert and the composite. Additionally, it has reduced the stress concentration by decreasing the angle between the liner and the insert.

With this geometry NGT succeeded to perform a pressure test up to 879 bar. At this pressure, no burst occurred but a leak was observed. Looking at the tank, it appears that the second layers of the composite has been extruded and pulled out of place.

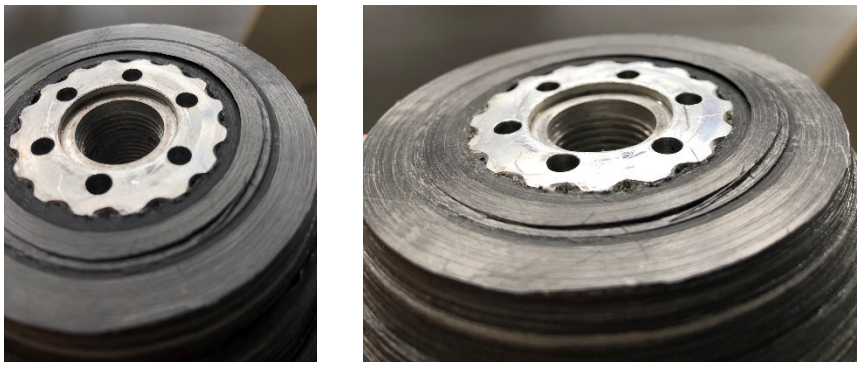

Figure 15: Extrusion of the first layer at 90°.

Based on this observation, NGT modified the design of the composite layers in the metal insert area. Thus, the geometry of the composite became:

By performing this modification, the tank reached 1235 bar during test pressure. With this performance, the tank prototype was able to reach a pressure of more than 3.5 times the operating pressure. However, the same extrusion issue observed before could be seen at 1075 but without leak. After that,

the extrusion of the layer becomes more and more pronounced until bursting occurs with the insert injection.

Extrusion of the 2sd layer

Figure 16 : Extrusion issue observed at 1206 bar and bust of the tank appeared at 1235 bar

In order to have a better comprehenssion of this result, this exactt geometry and fibre structure was simulated.

According to simulation, at 1235 bar the entire liner plastifies. However, Polymer F is a very ductile material that can achieve very high deformations. 160% of deformation can be reached at break according to the polymer supplier. For this geometry, only 25% of plastic deformation was calculated in the liner, espacially in the area near the insert. The material ensures watertightness in the tank and a geometry in which the composite can be applied. The pressure resistance is ensured by the composite.

On the other hand, by observing the simulation, it seems that the second highest stress level in the system appears in the composite structure, in the cylindrical area.

Then the simulation at 1235 bar shows an insert displacement of 2 mm, which is consistent with its ejection from the composite structure.

Following this observation, NGT proposed a new composite structure design in the metal insert region and in the cylindrical area to favor a break in the middle of the tank or at the end of the cone, it was envisaged to reduce the thickness of the layers at the cylinder part. This new prototype reached a burst pressure of 1101 bars with a hybrid failure mode in both the end-part and cylindrical area.

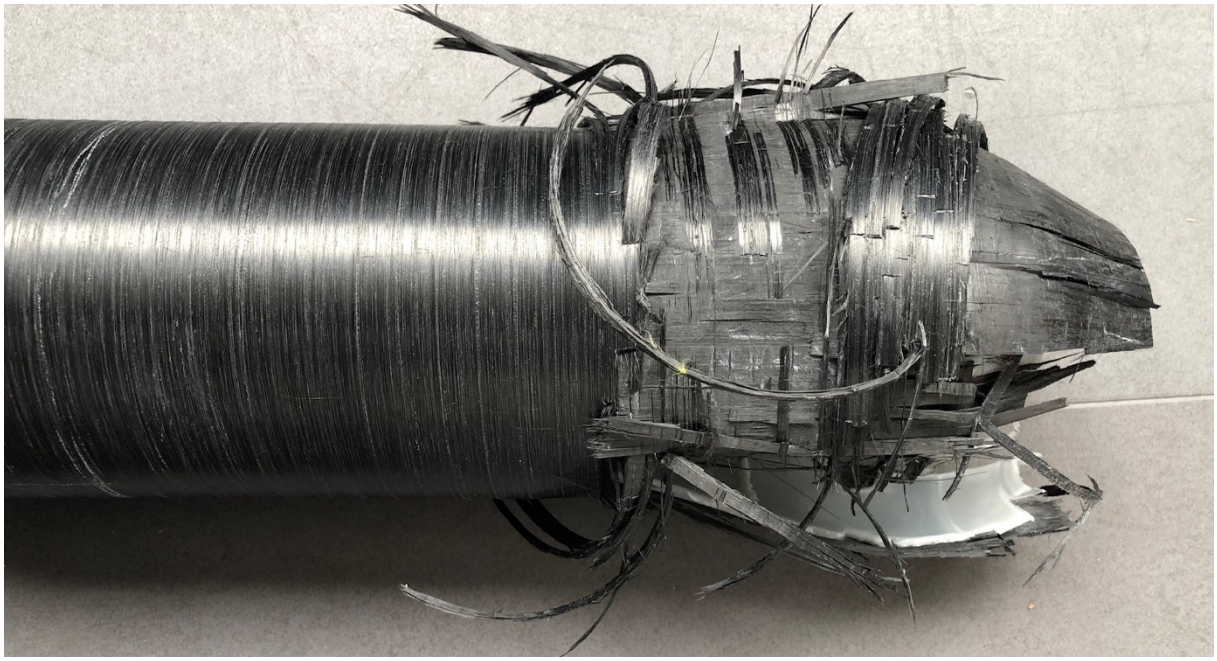

Figure 17: Prototype after burst at 1101 bar

The simulation model was fed with this specific prototype geometry to which a pressure of 1101 bar was applied. The simulation results showed:

- First, the whole liner plastifies. However, as explained above, this is not an issue. The plastic deformation observed is less than the 160% of deformation announced by the manufacturer.
- Secondly, looking at the second principal stress in the composite, it appears that the stress level in the hoop fibres at the end of the cone reaches the ultimate tensile strength claimed by the prepreg tape supplier.
- Thirdly, layer shear analysis revealed high stresses on the third layer at the end of the insert, but without exceeding the maximum values specified by the manufacturer (ILSS : 45 Mpa).

In general, the simulation model results are very consistent with experimental results and the model can be considered as very reliable.

Test at the operative and 1.5 x operative pressure

This was followed by 2 simulations: One simulation carried out at operating pressure, and another simulation at 1.5 x the operating pressure. The aim was to analyse the behavior of the tank for low pressure.

At the operating pressure (350 bar):

The liner is far from to plasticised as a whole, with the exception of the lip area. This is partly due to the geometry and contact conditions imposed. The results can be improved by smoothing the geometry of the insert and lip. However, again it is far from deformation at break. The composite is also far from its fracture zone. The longitudinal stress is less than 600 MPa and is reached on layer 2.

At 1.5 x the operating pressure (525 bar):

The equivalent stress in the liner is close to the elastic limit. The simulation measures a Von-Misses stress of around 30 MPa in the liner, with the exception of the area near the lip where it has already plasticised. In the liner, the plastic deformation is close to 5% in the affected zone.

Mass Balance

As a reminder, the tank is made up of a cylindrical part and two conical parts at the ends. An analysis of the mass distribution in the tank reveals the data shown in table 4 below:

	Insert	Composite	Liner
Volume [mm³]	69 864	225 595	91 102
Mass [g]	188,63	306,81	92,92
Internal volume [mm³]	526 135		
Total Mass [g]	588,37		
Total Mass [g]/ Internal volume [liter]	1 118		

Table 4 : Mass distribution in the conical section

To be able to consider tanks of different sizes, the data for the cylindrical part are expressed per millimeter in table 5 below.

Size per millimeter of cylinder	Composite	Liner
Volume [mm³/mm]	1862	1133
Mass [g/mm]	2,53	1,16
Internal volume [mm³/mm]	7776	
Total Mass [g/mm]	3,69	
Total Mass [g]/ Internal volume [liter]	474	

Table 5 : Mass distribution in the cylindrical section

By analyzing these data, it is possible to see that the distribution of mass is particularly important towards the start and the end of the tank. Improvements are possible in this area, particularly on the insert and the composite. These 2 parts represent respectively 32% and 52% of the total mass of the cone.

On the other hand, it is possible to note that this type of geometry is particularly interesting for long tanks. The ratio of mass per unit volume is much lower in the cylindrical part.

3 Mass Optimization

3.1 Composite reduction

Previous tests have resulted in a tank able to withstand a pressure greater than 3 times the operating pressure. However, the distribution of the composite in the tank is not optimised. By using the longitudinal stress as the failure criterion, it is possible to express the safety coefficient obtained on the tank along the axial position. This criterion gives an idea of the tank's local resistance. It is calculated from the maximum longitudinal stress: longitudinal stress at the x position / maximum longitudinal stress. Thus, by analysing the results at each composite layers, it is possible to obtain the following graph :

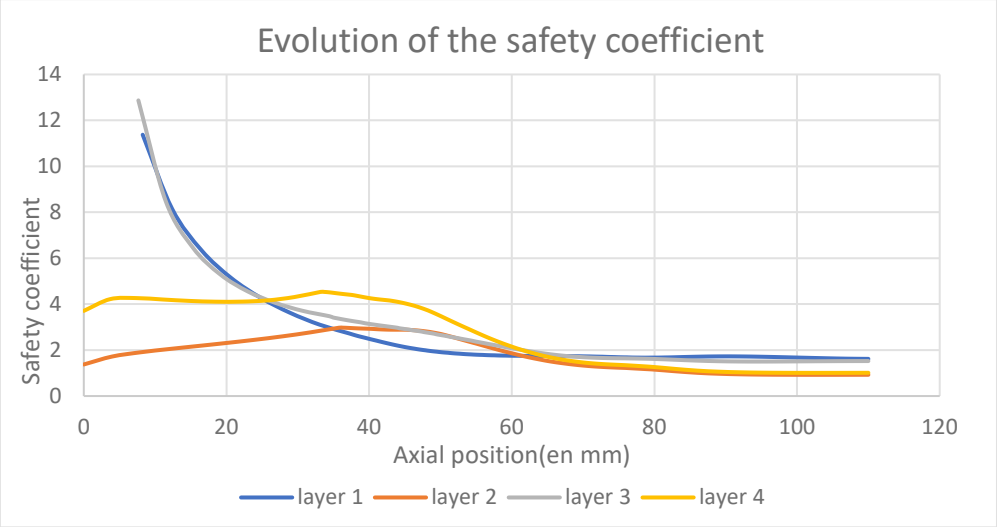

As the stress obtained is proportional to the thickness of the layers, it is possible to use the safety factor obtained on the layers to adjust the thicknesses. From the graph, it is noticeable that it is possible to adjust layers 1 and 3 of the composite at the end of the tank to reduce weight. Layer 4 can also be reduced because the coefficient s > 4. It might be beneficial to set a maximum value for s to avoid exceeding this limit, especially in the area near the end.

3.2 Insert modification

The potential mass gain is also possible by modifying the geometry of the insert. To improve the model, the pressure applied to the tank cap is transferred to the insert. A plastic model of the insert was also made.

After simulation, the insert appears to show signs of rupture at 1101 bar, at the level of the thread. This type of rupture has already been observed during pressure tests. This failure mode was first observed during the 1235 bar test. During this test, the thread on which the tank cap rested was ejected.

However, as long as the potential fracture zone is located close to the thread, solutions exist to avoid fracture.

Then, it was interesting to observe the evolution of stresses in the insert as the length of the insert decreased. 4 different geometries were tested with different insert length.

An area of high stress level and metal plasticisation appears close to the thread. The area becomes larger as the length of the insert decreases. The results showed that it would be difficult to reduce the length of the insert below 12 mm due to the presence of high stress zones other than those of the thread. The rest of the study was carried out on the 12 mm insert. The aim was to reduce stresses in the thread.

Several solutions exist to reduce the stresses in the insert. One solution is to try to rebalance the loads on the insert. To do this, the pressure in the tank can be used to redirect the forces applied to the insert. By shifting the thread of the insert, for example, the pressure is allowed to be applied radially to the insert. This effect results in a lower stress level. Another solution is to examine the expression of the load on the thread. This load is equal to the pressure x internal radius of the insert / (2 x the length of the thread). Thus, by increasing the length of the thread, the stresses in the insert can be reduced. this enlargement can be obtained by incorporating an extension in the insert. As a result, using both solutions in the insert has radically reduced stresses.

After the modifications made to the insert, the stresses on the thread have been reduced. The weight of the insert is 140g and the estimated gain on the tank is 142g.

4 WP3: materials characterization

4.1 Apparatus and materials

The machines that were used for characterization or specimen preparation are listed below.

- MTS 100kN traction and fatigue machine (EPFL, LPAC lab): traction on composite (Polymer A)
- Walter+Bai 100kN traction machine (Heig-VD, COMATEC institute): traction on composite (Polymer C), traction on polymer, NOL ring tests
- Shimadzu 20kN traction machine (Heig-VD, COMATEC institute): mode II toughness, ILSS, peel test, compression test
- JOOS LAP60 hot press (Heig-VD, COMATEC institute): composite plates fabrication

The main materials that were tested are the following.

- **Polymer A composite:** the hot-pressed plates were prepared as recommended by the supplier. Because of the press properties and thermal inertia, the processing cycles ended up being as follows.
  1. Temperature ramp up without pressure p=0 bar
  2. Final temperature ramp up with pressure p=15 bar
  3. Hold 5mn at p=25 bar
  4. Cool down up under pressure p=25 bar
  5. Release pressure until room temperature
  6. Open mold
- **Polymer C composite:** the hot-pressed plates were prepared at 35 bar.
- **Polymer E composite:** no reference available; no plates were produced with this material.
- **Polymer F composite:** no plates were produced with this material.

4.2 Traction (composite)

Method

Traction tensile tests on composites are based on the norm ISO 527-5. Although this norm applies to 0° and 90° composite layups, it was used to test [0°, 90°, 0°] layups to measure the best in-situ performances that can be achieved.

From the load-displacement relation, one can compute the plies longitudinal elastic modulus E_1 and the stress and deformation values at the onset of damage and at break. The displacements were measured using an extensometer and/or Digital Image Correlation (DIC) using a video microscope as well. The specimens were machined from the plates, sanded and cleaned with acetone, and fiberglass tabs were glued with Loctite 406.

Test results: Polymer A

Two layups were tested with this Polymer A-CF tape: [0°, 90°, 0°] and [90°, 0°, 90°] to bound the properties of the actual layup. Five specimens of each were machined and the test followed the parameters

recommended for the norm for 0° layups. Each layup has one half of the plies at 0° and the other half at 90°. The total thickness of the plate is 1.9mm.

The specimens exhibit a clear delamination before complete failure, as shown in Figure 32. The resulting properties are presented in Table 6. The effective elastic modulus of the UD composite could be estimated with a linear fitting between 0.5% and 1% deformation and based on a linear rule of mixture without confinement and Poisson effects. The computed stress is the laminate mean stress.

In simulations, the failure criterion used is often the fibre deformation. It is assumed that when delamination occurs, the tank bursts. So the value of 1.3% was usually used because there are many factors that may induce variations from these tests:

1. The actual layup is different and with different thicknesses.
2. Unlike here, the stress state is bi-axial.
3. The process is different; one can expect the properties measured here with an optimized tape deposition process.

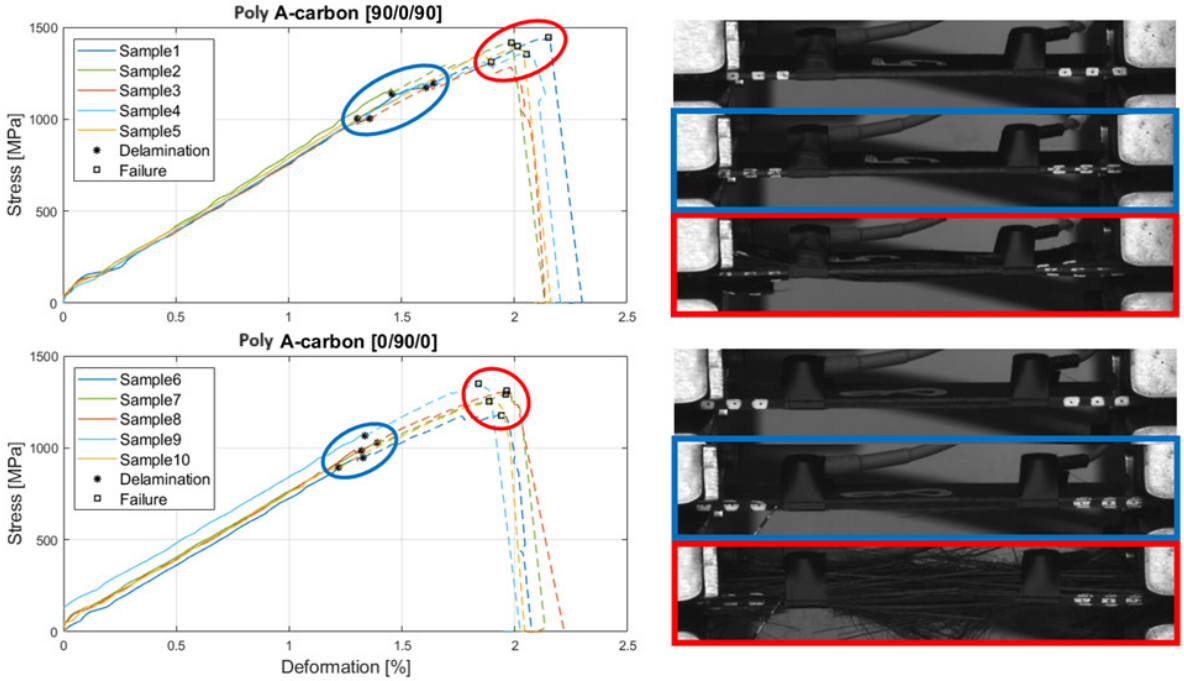

Figure 18: results: traction on Polymer A composite

Table 6: results summary: traction on Polymer A composite

	[90/0/90]	[0/90/0]
Elastic modulus E1 [MPa]	142	138
Strain at delamination [%]	1.49	1.31
Strain at break [%]	2.02	1.92
Stress at delamination [MPa]	1104	984
Stress at break [MPa]	1384	1276

Test results: Polymer C

This test was very similar to the previous one for Polymer A with one set of six [0°, 90°, 0°] specimen machined from a 2.18mm thick hot-pressed plate. In this test, delamination did not appear as clearly as it did for the Polymer A composite, so only the complete failure properties were measured.

On the other hand, transverse cracks appear in the 90° layer much sooner that failure (Figure 33); it is difficult to measure the exact value, but generally between 0.4% and 0.7% deformation. From these results, the maximum deformation of the 90° embedded in 0° plies must be expected around 0.5%, while the datasheet predicts 0.26% deformation for a 90° laminate. It shows that alternating layers to embed 90° is beneficial for this application, but it also confirms that Polymer C is brittle in the transverse direction.

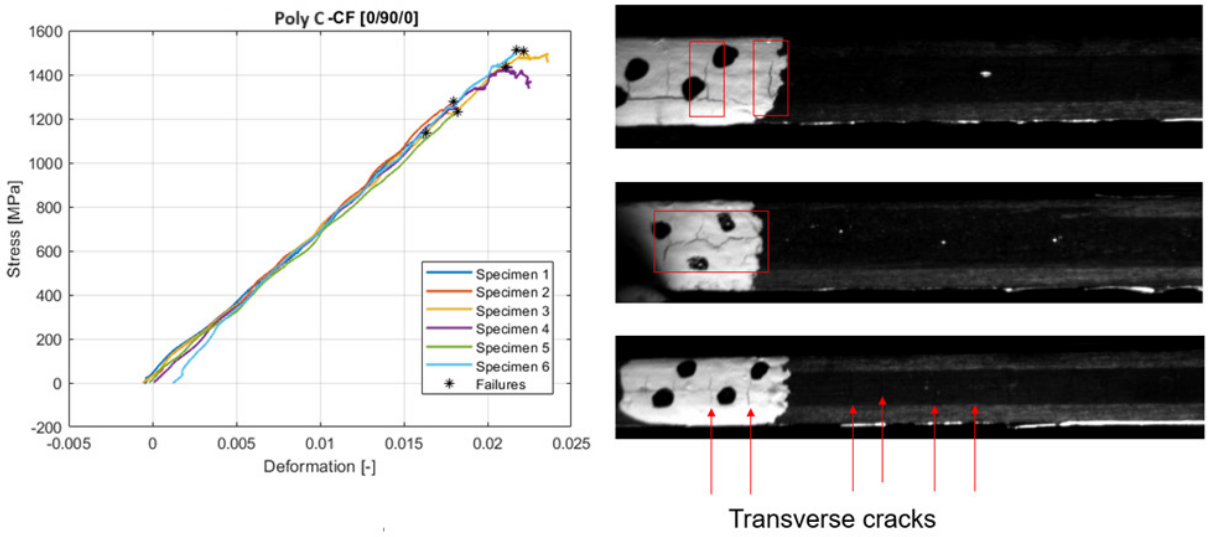

Figure 19: results: traction on Polymer C composite

Table 7: results summary: traction on Polymer C composite

	[0/90/0]
Elastic modulus E1 [MPa]	131
Strain at break [%]	1.96
Stress at break [MPa]	1393

4.3 Traction (polymer)

Method

This test is based on the norm ISO 527-2. It characterizes the strength of the welding joint after assembling the different parts of the liner. The specimens were laser cut from a tube in the longitudinal direction, in order to place the weld transversely to the direction of loading. To compare the results to the healthy polymer, dog bone shaped specimens were cut from the same tubes without welding joint. The dog bone shape is necessary to avoid breaking in the jaws, unlike the welded specimens which always break at the joint.

Since specimens are cut from a tube, they are curved in one direction. A static simulation allowed ensuring that crushing their tips in the machine jaws does not cause too much stress variation in the middle part. The standard deviation of the Von Mises equivalent stress in a cross section turns out to be 5.3% of the mean stress, which is acceptable (Figure 34).

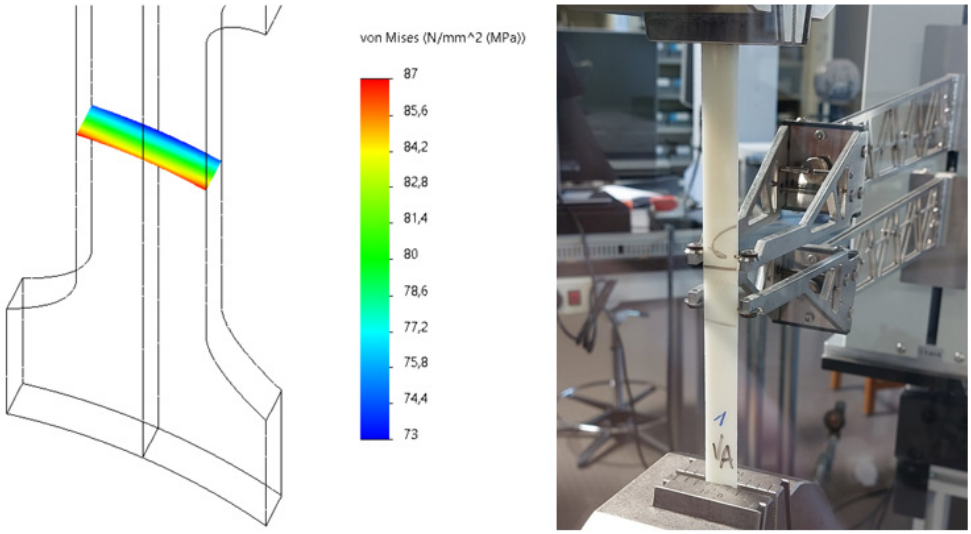

Figure 20: characterization of welding joints

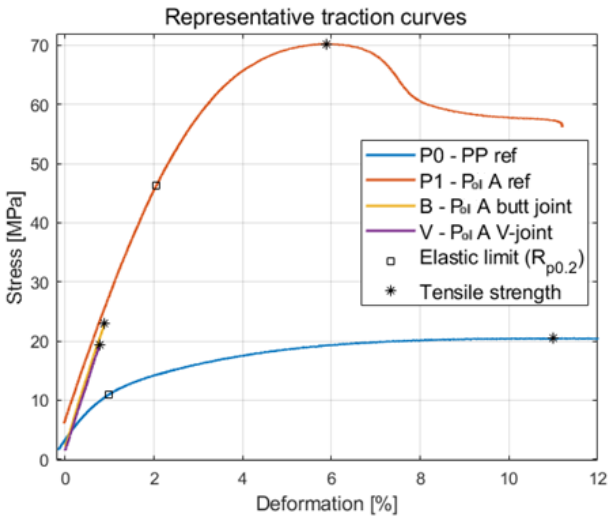

Figure 21: representative load-displacement curves

Test results: Polymer A

The 35 shows representative test results. Non-welded PP was tested as well to setup the test and make another baseline. The results show that failure of welding joints is completely brittle, even if the material itself is ductile. V-joints were tested with different conditions defined by NGT in terms of applied pressure, rotational velocity and contact time. The results are shown in 36 and show that the best specimens, for instance the "VC", could reach Polymer A's yield stress.

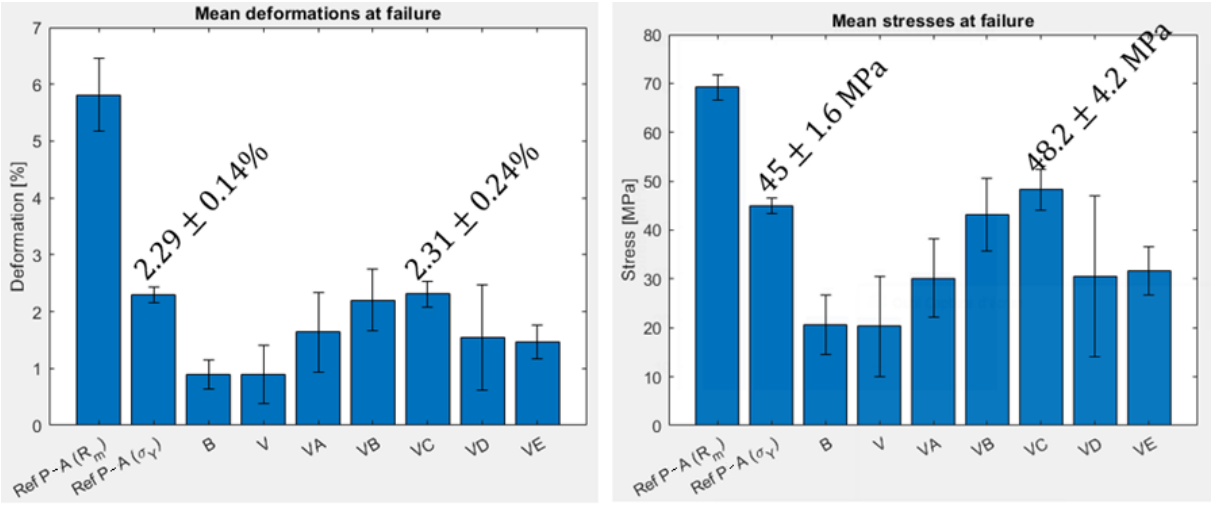

Figure 22: results of welding joints characterization (Polymer A)

Below are shown the test results of the next set, which was defined by NGT. The testing conditions depends on welding parameters such as spinning speed, shape of the profile, etc. The best parameters remain those used to make the "VC" specimens of the previous set of tests.

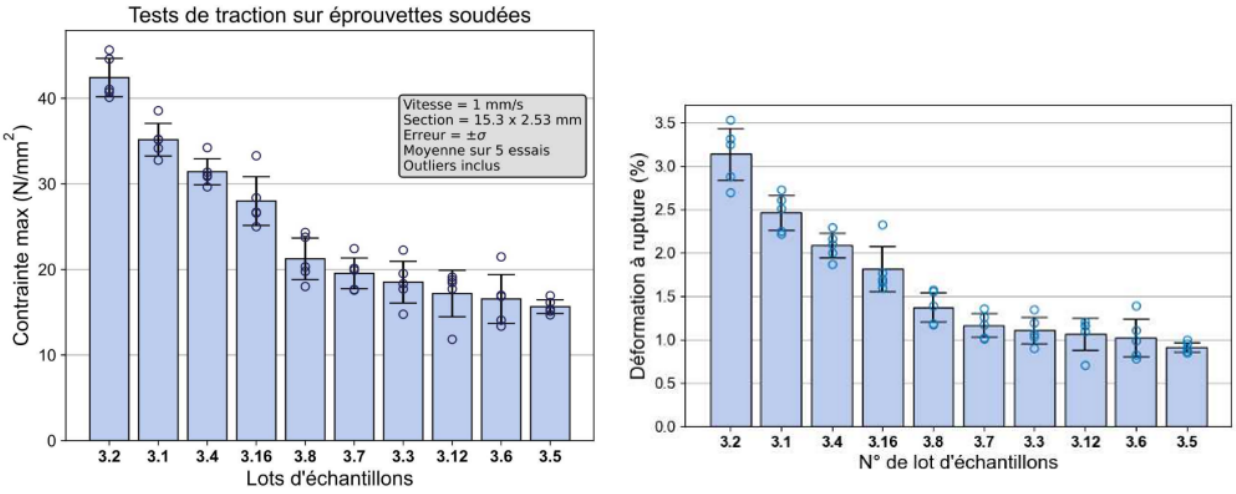

Figure 23: results of welding joints characterization (Polymer A, 2nd set)

Test results: Polymer C

Four Polymer C grades were tested, with different welding conditions and material reference. Below are the results. The Polymer C grade, which turns out to be the best candidate for welding is the 4th one because the joint resistance reaches de polymer resistance. However, note that the healthy polymer is also very brittle, which is typical of Polymer C.

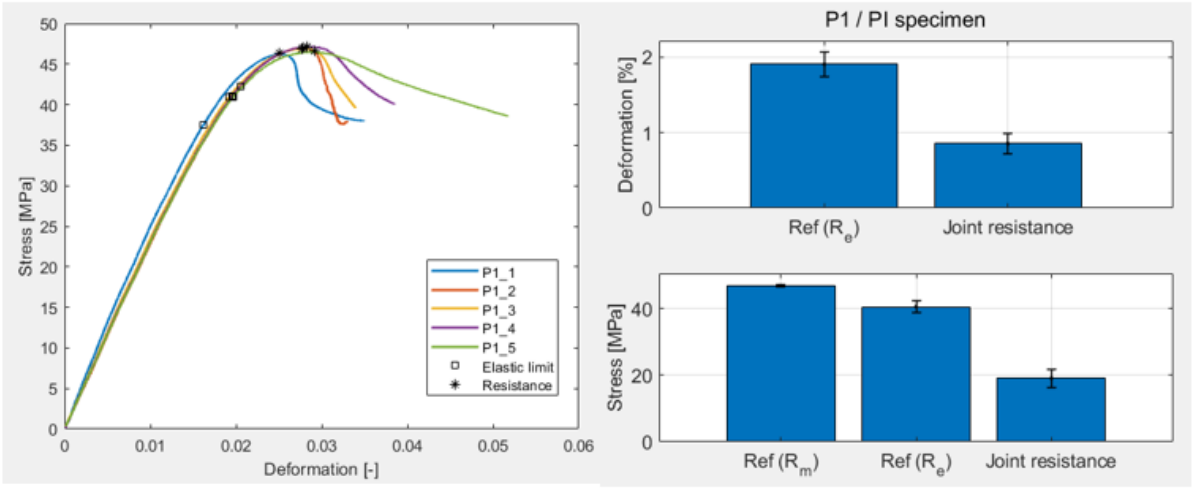

Figure 24: results (Polymer C - 1)

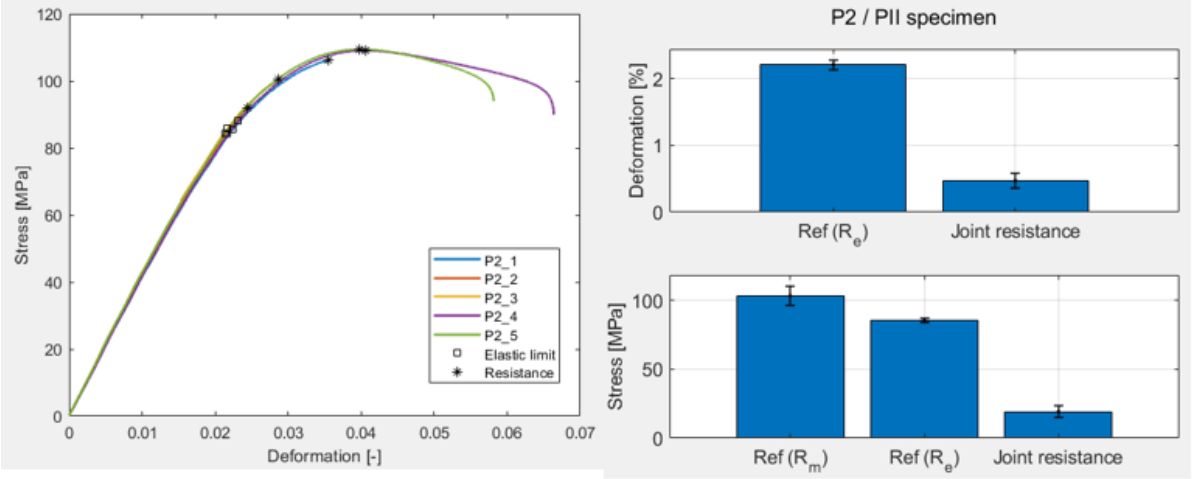

Figure 25: results (Polymer C - 2)

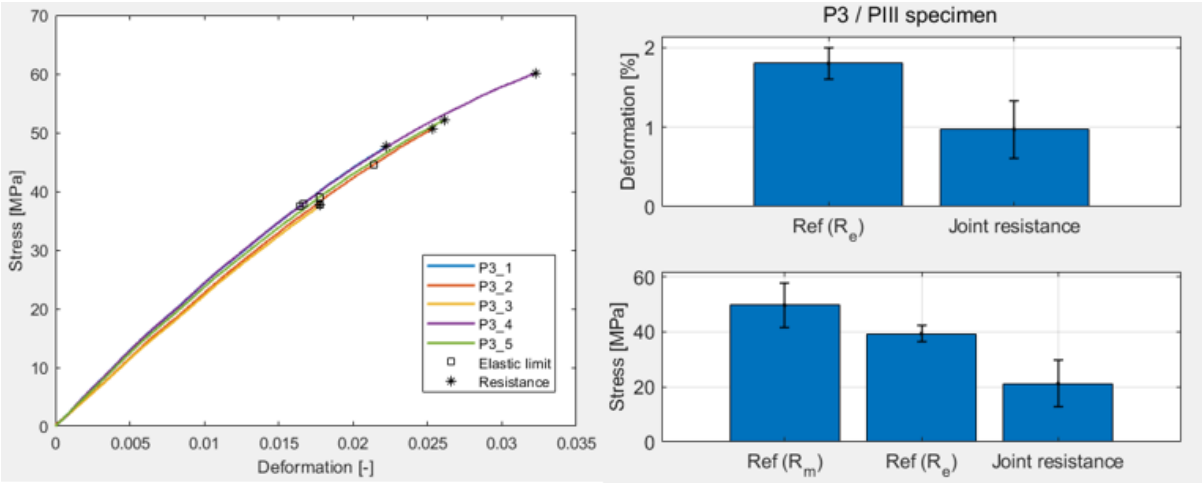

Figure 26: results (Polymer C - 3)

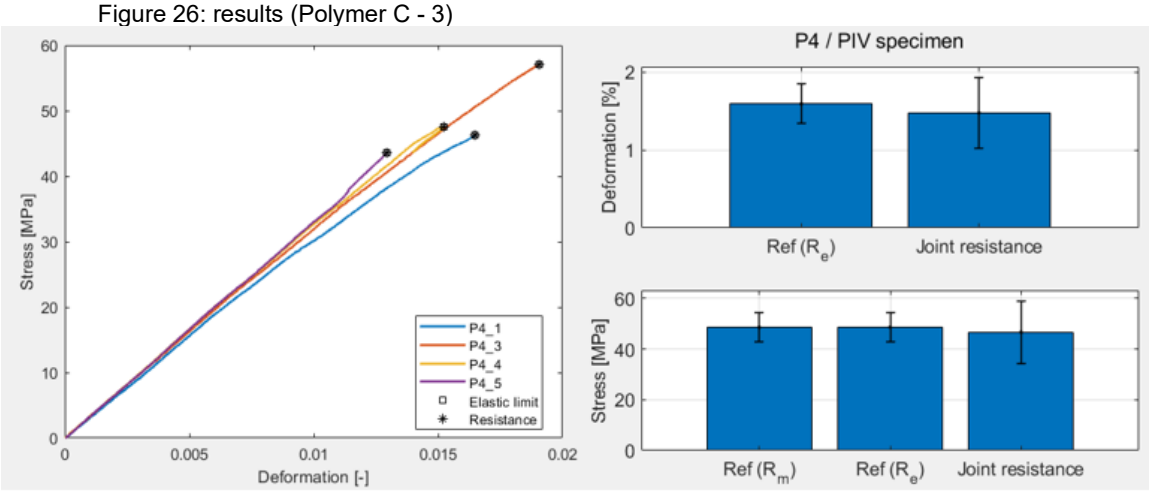

Figure 27: results (Polymer C - 4)

4.4 Compression test

Method

Compression tests were done to analyze the compressive elastic-plastic behavior of the liner. Polymers undergoing a highly hydrostatic stress state are expected to have different failure mechanism and properties than what a simple tensile provides.

The specimens are rectangular plates, about 10mm wide and 2-4mm thick. A constant velocity of 0.1 mm/s is applied to a moving plate to compress the specimen. The velocity is very low to minimize viscoelastic effects. Moreover, the test is paused at different stress levels to allow the polymer to relax: one minute at 50MPa, 80MPa and 120MPa. The tests were ended at 150MPa.

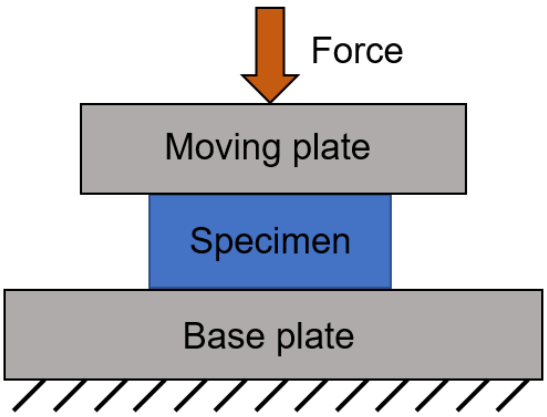

Figure 28: compression test description

Test results: Polymer A, Polymer B

The tested materials are Polymer B, Polymer A grade 1 and Polymer A grade 2. Their dimensions are detailed in Table 8. Polymer A grade 1 just had a slightly different loading cycle from the one explained above: no relaxation at 50MPa, 3mn pause at 80MPa and 1mn pause at 120MPa.

Table 8: compression test; specimen dimensions

	Width	Depth	Thickness
Poly A grade 1	9.2	9.7	2
Poly A grade 2	9.92	9.95	3
Poly B	10	11.85	4.05

The results are presented in figure 43. There is also an example of how the behaviour of polymers was modelled once plasticity was implemented in the FE model. We know from the supplier's datasheet that Polymer B has a Young's modulus of 2470 MPa and a yield stress of 63 MPa. So the measured deformation is scaled to match this data and get rid of sources of error. Errors mainly come from:

- **Specimen size:** the effective Young's modulus varies with the size of the specimen because of confinement effects and incompressibility.
- **Friction:** friction prevents the specimens from deforming freely laterally; it tends to increase the stiffness.
- **Machine stiffness:** the stiffness measured is the stiffness of the machine in series with the stiffness of the specimen.

The resulting work hardening value for Polymer B is 264 MPa.

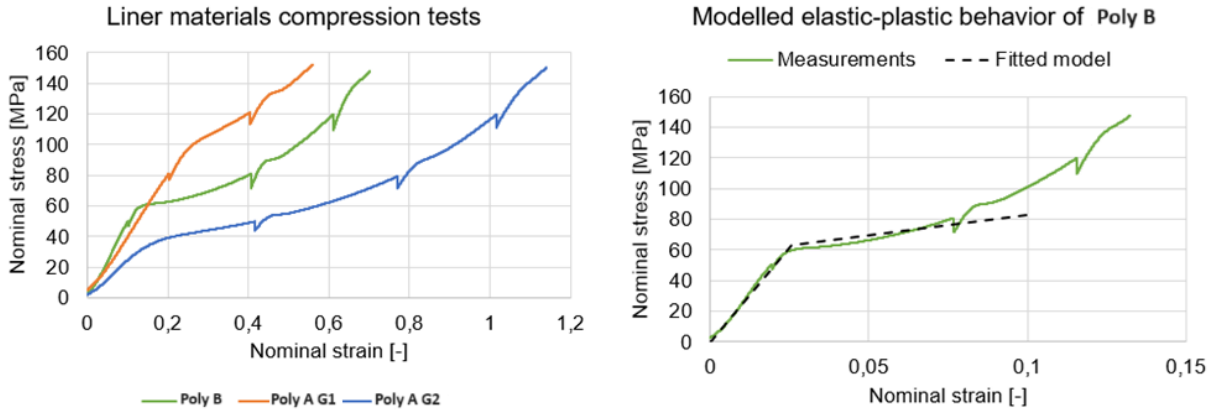

Figure 29: compression tests results

4.5 Mode II toughness (G_{IIc})

Method

This test allows measuring the mode II toughness of [0°, 90°, 0°] laminates. It is based on the compliance method used in [3] and [4] and adapted to multi-directional composite layups. During the three-point bending test, an initiated crack propagates either in the 90° layer, or at the 0°/90° interface. At every propagation point, the specimen compliance C increases and the associated crack length a is recorded. The goal is to find the best-fitting compliance curve $C(a)$ based on the critical states, in other words just before a propagation happens.

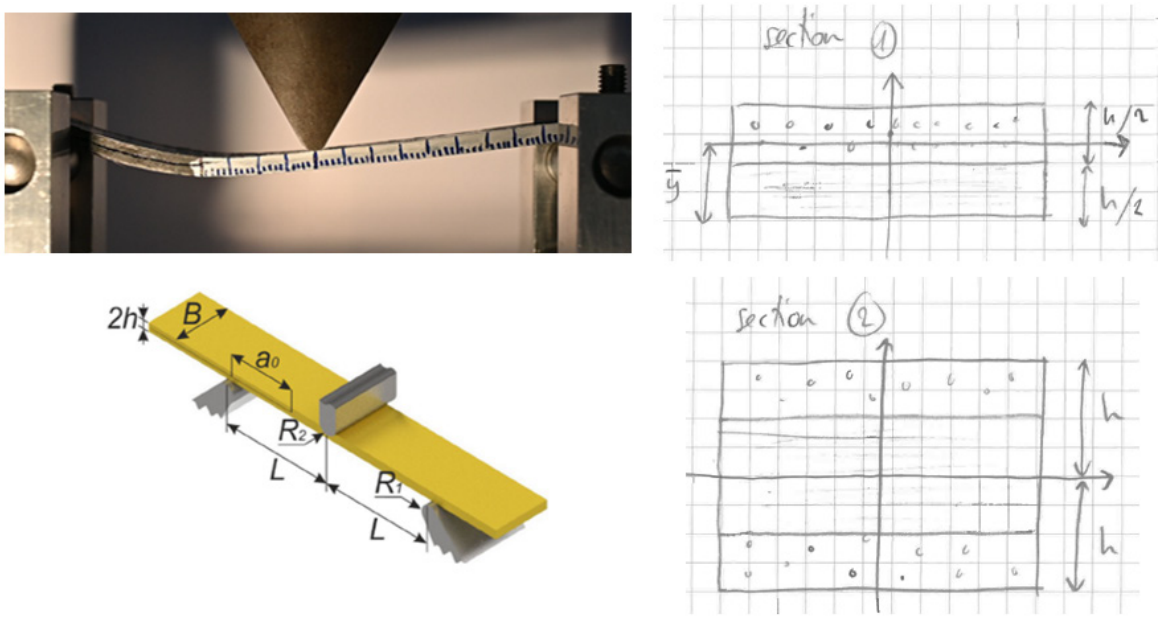

Figure 30: mode II toughness characterization

The compliance of the specimen can be expressed $C(a) = C_{th}(a) \cdot \alpha$ with the theoretical compliance derived from beam theory

$$C_{th}(a) = \left(\frac{1}{24(EI)_1} - \frac{1}{12(EI)_2}\right) a^3 + \frac{L^3}{6(EI)_2}$$

and the constant α taking defaults and nonlinearities into account, found by setting $C(a_0) = C_{th}(a_0) \cdot \alpha$. The subscripts 2 refer to the [0°, 90°, 0°] fully consolidated laminate and the subscripts 1 refer to the upper or lower half of the laminate, for the section of the beam that is delaminated. Then, the mode II toughness G_{2c} is derived from the fitted compliance by evaluating the energy release rate (ERR) at the propagation points. The ERR is

$$J_{II} = \frac{P^2}{2B}\frac{\mathrm{d}C}{\mathrm{d}a} = 3\alpha\left(\frac{1}{24(EI)_1} - \frac{1}{12(EI)_2}\right) a^2 = G_{IIc}$$

with P the force applied. This formula actually describes the ERR (J-integral value) in general, and is equal to G_{IIc} at propagation points. This is how the latter can be determined.

The specimens were machined from a 3.25mm thick hot-pressed plate. The pre-crack was introduced using a folded aluminum sheet placed in the center of the laminate during its preparation. To end up having an actual crack, the pre-cracks were manually propagated in mode I for a few millimeters. The dimensions of the specimen are $L = 50\text{mm}$, $a_0 = 30\text{mm}$, $B = 25\text{mm}$ and $2h = 3.25\text{mm}$ (see Figure 44). The loading rate is 2mm/mn.

Test results: Polymer A

Results are shown in figure 45. Each color represents a specimen, circles are for 0°/90° cracks and triangles are for 90° cracks, which were treated separately. Apart from two outliers, the compliance fits very well the measurement points. The toughness exhibits a rising crack growth resistance curve (R-curve), probably thanks to the rough profile of the crack surfaces, which prevents them to slide

against each other and make the crack propagate. So this R-curve tends to make crack propagations stable.

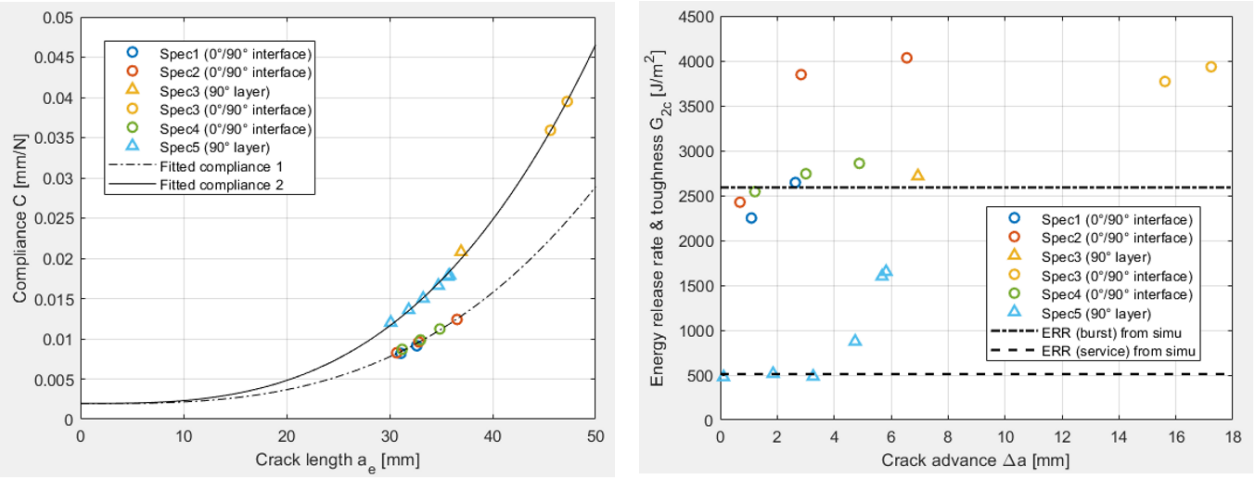

Figure 31: G2c results (Polymer A)

The dashed lines represent the ERR of a tank at service and burst pressure. It was determined using simulation by calculating the total elastic energy U for several crack lengths a placed in the critical zone, *i.e.* at the cone-cylinder transition region. The energy release rate is then calculated as

$$J_{II} = \frac{\partial U}{\partial a}\Big|_p$$

with p the applied pressure, either the service or the burst pressure. The results show that initial defaults may propagate in a stable way and then be stopped by the increasing toughness. These results are used as simulation inputs for the nonlinear cohesive FE model (see Crack propagation).

Test results: Polymer C

The same analysis was done for Polymer C-CF specimens. The compliance curve fits very well too. The toughness is higher than Polymer A with a lower increase with crack advance. For cohesive simulations, the lowest values of toughness are generally used for safety. Here, 1kJ/m^2 would be a reasonable value.

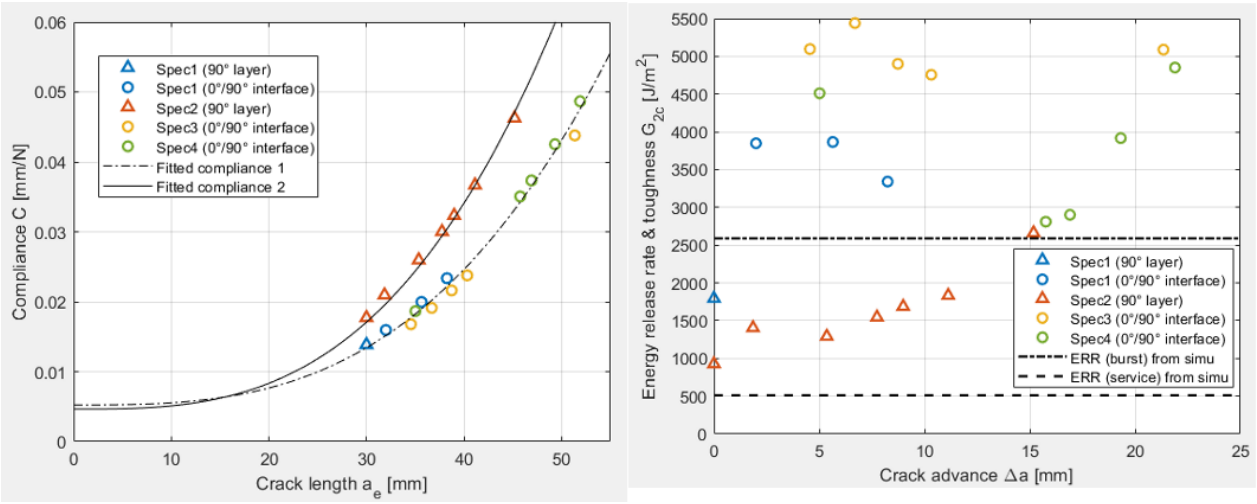

Figure 32: G2c results (Polymer C)

4.6 Interlaminar Shear Strength (ILSS)

Method

ILSS tests follow the norm ASTM D 2244. The ILSS of a composite is a good indicator of its quality. The closer the ILSS is to the supplier's datasheet value, the better the process is. Many tests were done to evaluate the quality of NGT's process and to know the in-situ strength of the composite. They were done on hot-pressed plate to measure the largest achievable value (comparable to the datasheet), and on specimens, which were cut from a winded ring produced by NGT. The latter were based on the Naval Ordnance Lab (NOL, see [5]) to test curved specimens.

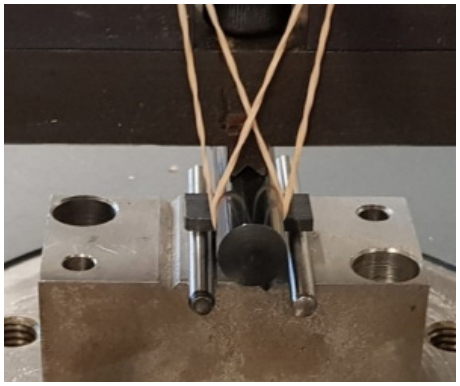

Figure 33: ILSS test

Usually, the largest force F of the load-displacement curve is used to compute the ILSS as

$$\text{ILSS} = \frac{3F}{4bh}$$

where b is the width and h is the height of the specimen. When the peak force appears at a large displacement ($> \sim 1$mm), which happens for ductile materials, the onset of damage was recorded as well. It was defined either when the loading curve was not linear anymore, or when the first force drops were observed.

Test results: Polymer A plate and first NOL tests

The first tests were done on Polymer A-CF. The results for a hot-pressed plate and for NOL tests are shown in48. The in-situ ILSS only reaches about the half of the ILSS from a well consolidated plate. It is an indicator that large improvements should be made on the process.

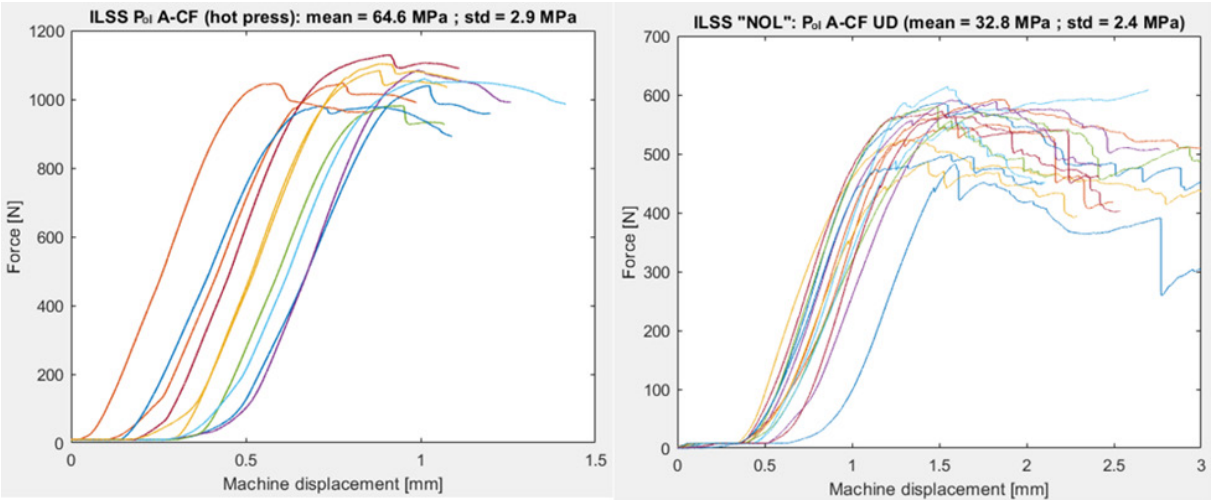

Figure 34: ILSS results (Polymer A)

Test results: Polymer C plate and Polymer A, Polymer D, Polymer C NOL tests

The next tests were done on several composites with different processing parameters, which were known by NGT only. The results are shown in 49 where a representative curve of each specimen type is used for comparison. The specimen types are:

- **Polymer C:** hot-pressed Polymer C-CF plate
- **NOL-R1, NOL-R2:** Polymer A-CF with different tape tension values
- **NOL-R3:** Polymer D-CF
- **NOL-R4, NOL-R5:** Polymer C-CF with different values of depositing velocity (*i.e.* thermal power supply)

The process for Polymer A-CF was highly improved since the first tests: the ILSS increased from 33MPa to 46MPa. As for the Polymer C-CF, the in-situ ILSS is only about 38MPa while the plate ILSS is 57MPa. Interestingly, processing parameters of the NOL-R4 specimens made a much more ductile Polymer C-CF composite than the ones of the NOL-R5 specimen.

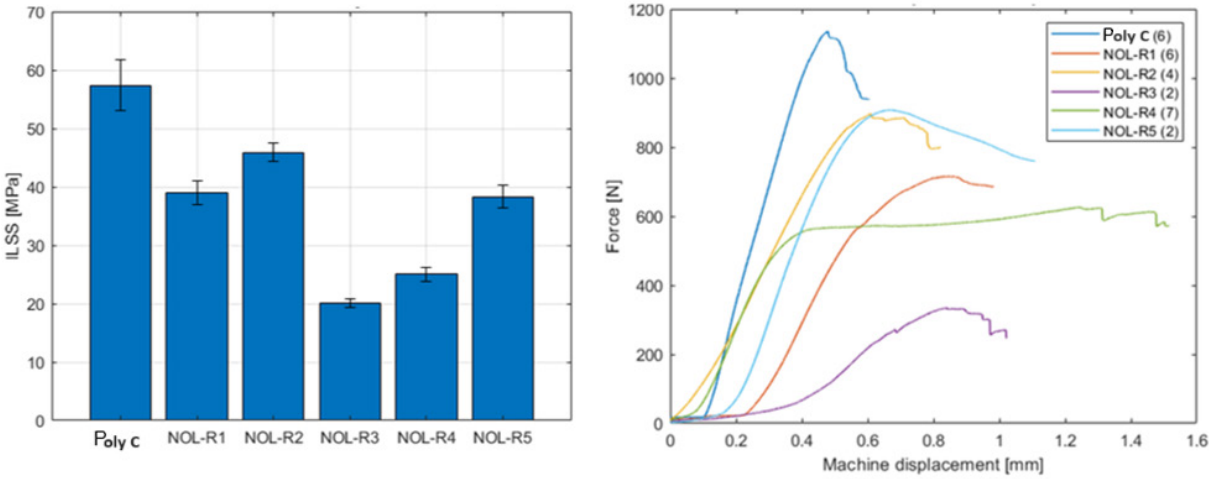

Figure 35: ILSS results (composites with Polymer A, C and D)

Test results: Polymer F NOL tests

Finally, NOL tests were done on two Polymer F-CF rings with different tension values. One can observe that the second ring, with more tension, was able to reach 45 MPa in terms of maximum shear, which equals the value given in the supplier's data sheet. It quantitatively confirms NGT's observations that Polymer F is easier to process than Polymer A.

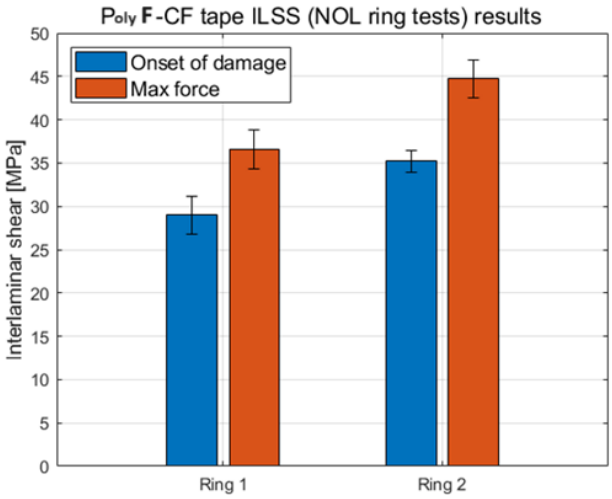

Figure 36: ILSS results (Polymer F)

4.7 NOL ring tests

Method

NOL ring tests [5] are tensile tests performed on a ring specimen and allow measuring the in-situ properties of the composite once processed, in this case with NGT's technology. It is particularly useful to determine the achieved resistance of the composite, the stiffness or effective modulus being not very sensitive to the process. The results may not exactly reflect the situation of a pressurized tank because of the bending that can be introduced in the loading zone (Figure 51, red circle). Locally, the machine pulls straight on a portion of ring that has obviously some curvature. So the values of resistance obtained can be slightly underestimated.

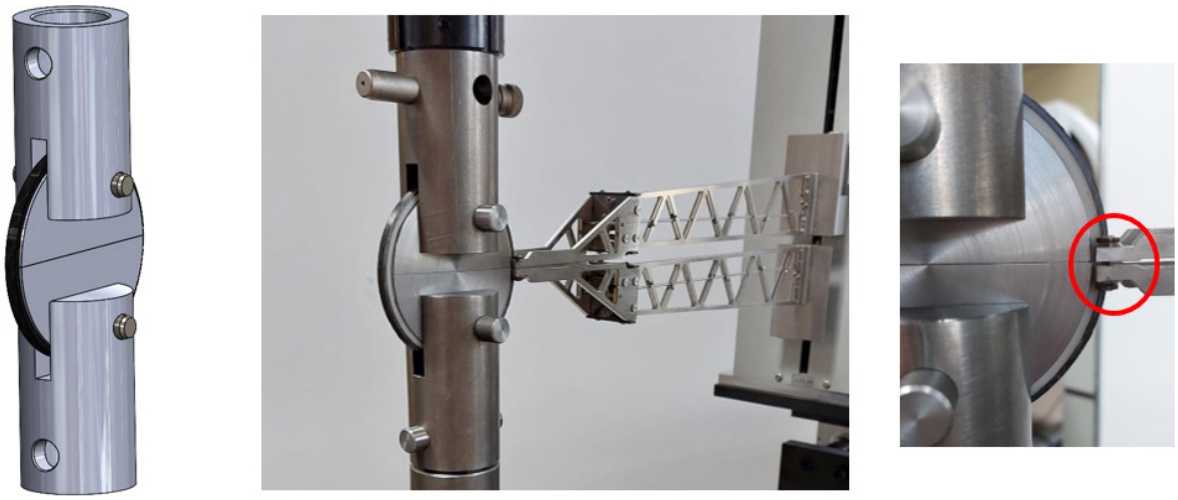

Figure 37: NOL ring test

Test results: Polymer A

Eight Polymer A-CF unidirectional specimen were tested with the following dimensions:

- Width 6.35mm
- Composite thickness 2.3mm
- Liner internal diameter 102mm

The extensometer slipped during three tests. This is why the deformation (Figure 52, top) is not well calculated in these cases. Anyway, due to friction, the ring is not loaded homogeneously, so it is not possible to accurately measure the longitudinal elastic modulus.

On the other hand, the resistance was measured at 1200 MPa with a standard deviation of 11%. This value is very low: using the results of the traction tests (see 4.2 Traction (composite)), it leads to a deformation of 0.86%. To conclude, we estimated that these tests were not the best to evaluate the quality of the process as opposed to NOL ILSS tests. So other NOL ring tests were done.

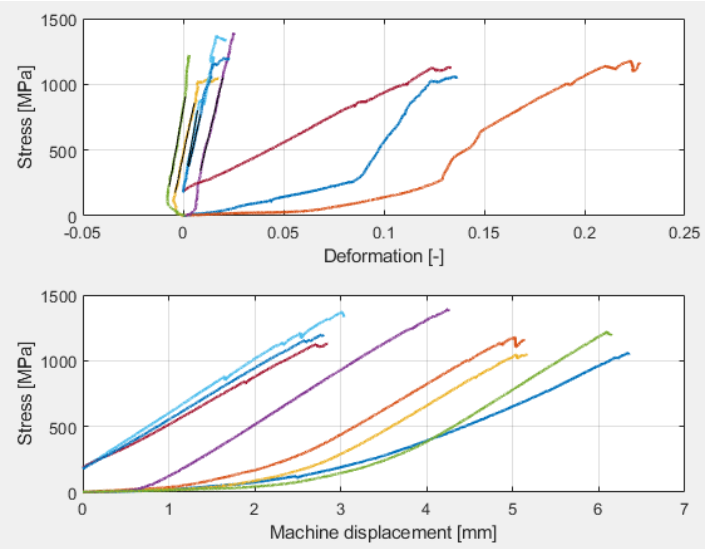

Figure 38: load displacement curves of NOL tests

4.8 Peel tests

Method

A peel test setup was developed to characterize the adhesion quality of longitudinal composite tapes. A tape is pulled using a traction machine at a velocity of 20mm/mn. The peeling force is measured and averaged, and is used mainly to compare different processing parameter sets. The tests carried here were done either on tapes, which were deposed on a portion of liner by NGT. Thanks to the size of the lever arm, the vertical force applied by the cylindrical liner on the aluminum base plate is much smaller than the peel force. Therefore, while the cylinder slides on the plate, the friction force is negligible. Moreover, a PTFE layer was glued to the plate to reduce friction more. The tapes are 12mm wide and 0.2mm thick et the PU roller has a diameter of 20mm.

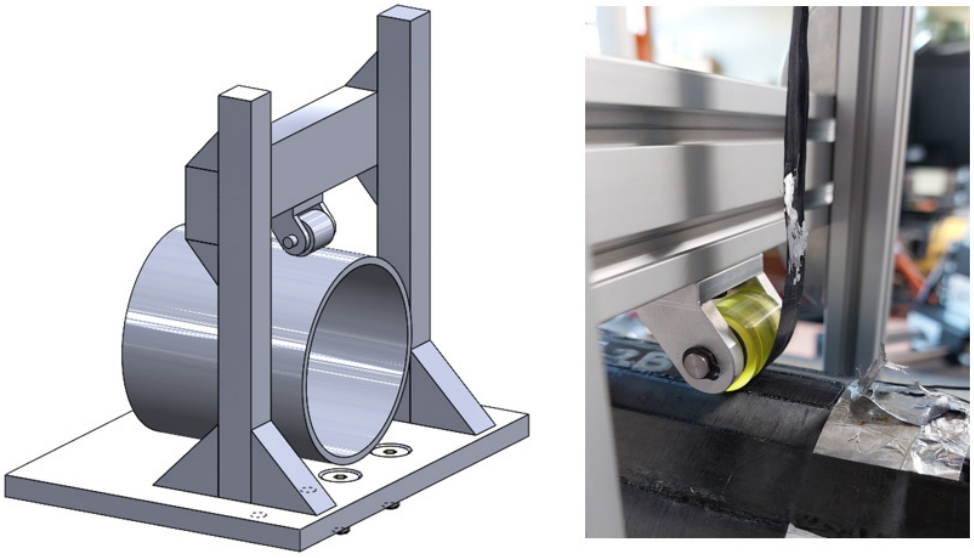

Figure 39: peel test

Test results: Polymer C

The processing parameters that were tested were the applied pressure on the deposited tape and the velocity of deposition. All parameters are detailed in Table 9.

Table 9: peel test parameters (Polymer C)

Test reference	Liner material	Tape	Conformation roll pressure (bar)	Linear speed tape 1 (mm/s)	Comment
1-2B	Poly 4	CF-Poly C	2	15	
2-2B	Poly 4	CF-Poly C	2	10	Gros bourrelet devant le rouleau
3-2B	Poly 4	CF-Poly C	2	20	
1-3B	Poly 4	CF-Poly C	3	15	

An example of load-displacement curve and the results summary are shown in54. In this example, the force is averaged between about 15mm and 60mm of machine displacement. The results show that applying a pressure of 2bar at a speed of 10mm/s is the best parameter combination among the tested ones for Polymer C-CF composite deposited on “Poly 4” liner.

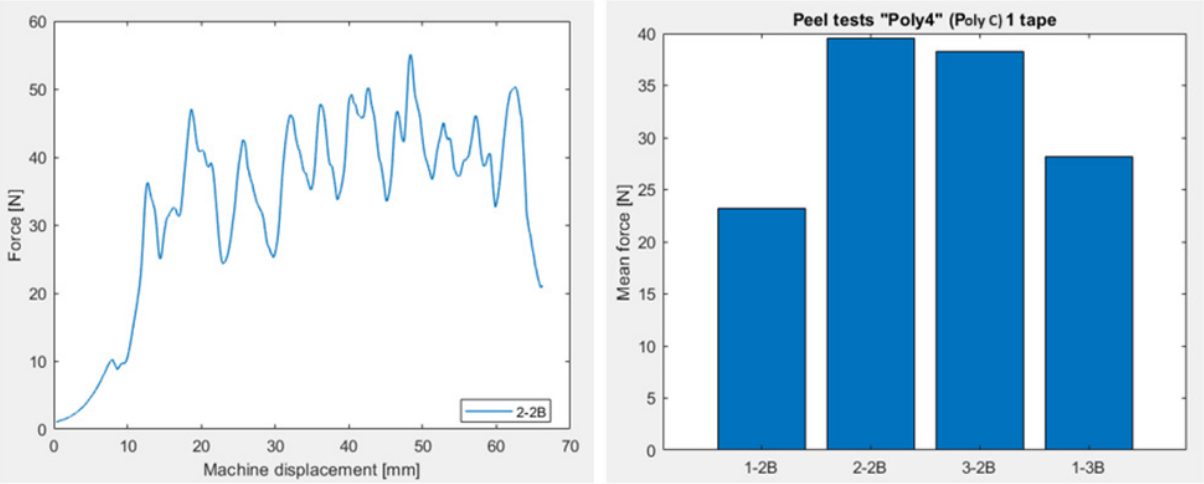

Figure 40: peel test (Polymer C); example of load-displacement curve and mean peel forces comparison

Test results: Polymer A

Like for Polymer C, the tested parameters for Polymer A are detailed in Table 10.

Table 10: peel test parameters (Polymer A)

Test reference	Liner material	Tape	Conformation roll pressure (bar)	Linear speed tape 1 (mm/s)	Comment
1-2B	Poly 3	CF-Poly A	2	12.5	
1-3B	Poly 3	CF-Poly A	3	12.5	
1-4B	Poly 3	CF-Poly A	4	12.5	
1-2B	Poly 1	CF-Poly A	2	12.5	Gros bourrelet devant le rouleau de dépose
2-2B	Poly 1	CF-Poly A	2	20	Bourrelet devant le rouleau de dépose
3-2B	Poly 1	CF-Poly A	2	25	Pas de bourrelet visible mais tape bien imprimé dans le liner
3-4B	Poly 1	CF-Poly A	4	25	

The results in Figure 5555 show that applying a pressure of 2bar at a speed of 12.5mm/s is the best parameter combination among the tested ones for Polymer A-CF composing deposited on “Poly 1” liner. Likewise, the best parameter combination for “Poly 3” liner is 3bar of pressure and a velocity of 12.5mm/s.

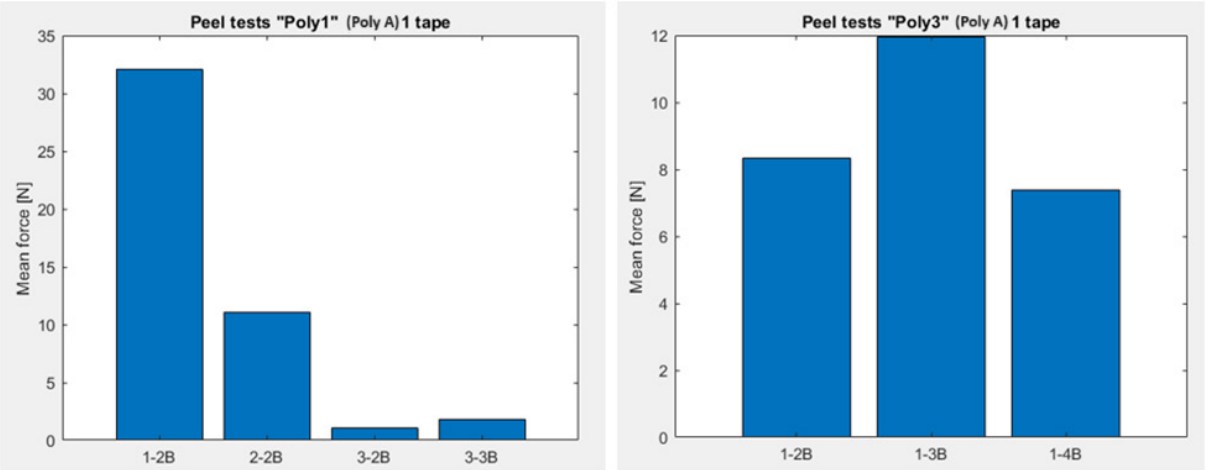

Figure 41: peel test (Polymer A); mean peel forces comparison

5 References

[1] Charan, V. S., Vardhan, A. V., Raj, S., Rao, G. R., Rao, G. V., & Hussaini, S. M. (2019). Experimental characterization of CFRP by NOL ring test. *Materials Today: Proceedings*, *18*, 2868-2874.

[2] Farmand-Ashtiani, E., Alanis, D., Cugnoni, J., & Botsis, J. (2015). Delamination in cross-ply laminates: Identification of traction–separation relations and cohesive zone modeling. *Composites Science and Technology*, *119*, 85-92.

[3] Fernandes, R. M. R. P., Chousal, J. A. G., De Moura, M. F. S. F., & Xavier, J. (2013). Determination of cohesive laws of composite bonded joints under mode II loading. *Composites Part B: Engineering*, *52*, 269-274.

[4] Gliszczynski, A., & Wiącek, N. (2021). Experimental and numerical benchmark study of mode II interlaminar fracture toughness of unidirectional GFRP laminates under shear loading using the end-notched flexure (ENF) test. *Composite Structures*, *258*, 113190.

[5] Kinna, M. A. (1964). NOL Ring Test Methods. United States naval ordnance laboratory, with oak, Maryland, NOLTR, 64-156.

Appendix B

Work package 6 “Pressure tanks recyclability assessment”

July 2024

Authors:

David Choffat, Prof. Bruno Bürgisser

Agenda

1. Découpe des réservoirs
2. Broyage
3. Séparation des broyats
4. Compoundage
   a) Du volume hétérogène
   b) Du volume séparé
5. Injection
6. Essais de traction
   a) Réservoir en carbone + PP
   b) Réservoir en carbone + N5H
7. Conclusion

1. Découpe des réservoirs

- 2 types de réservoirs :
  - Carbone + PP
  - Carbone + **Polymer A**
- Apparition d'un décollement des fibres
  - Défaut de production ?

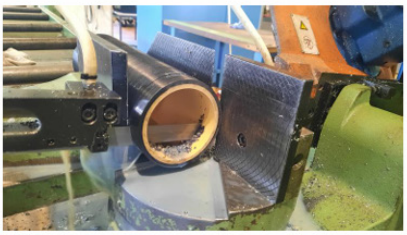

Réservoir en Carbone + PP (PP CF)

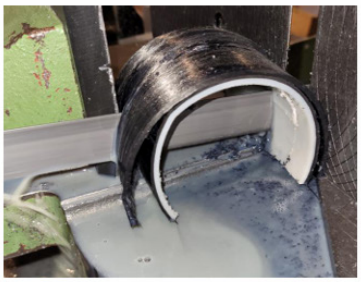

Réservoir en Carbone + **Polymer A**

3

2. Broyage des morceaux coupés

- Broyage dans concasseur «Rapid®»15
  - Entre 3 et 7% de pertes dans le procédé (1560g PP CF => 1432g) (1746g Poly A =>1705g)

4

3. Séparation des broyats PP CF

- 1400g de PP CF ont été divisé en deux volumes de 700g
- Pas de décantation avec les broyats Polymère A - CF
  - 1 volume conservé en mélange hétérogène
  - 1 volume séparé par décantation en 4 répétitions

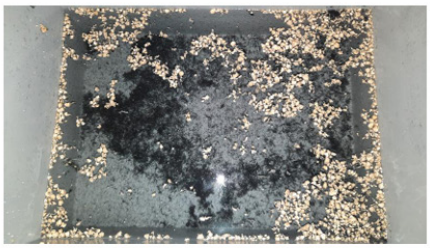

5

3. Séparation des broyats

700g de volume hétérogène PP CF

284g de Polypropylène

414g de tape Carbone-PP

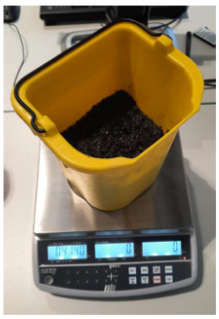

1705g de Poly A - CF

700 + 284 + 414 = 1398g => 12,5% de pertes par rapport à la masse de départ

6

4. Compoundage du volume hétérogène

- Design des vis d'extrusion :

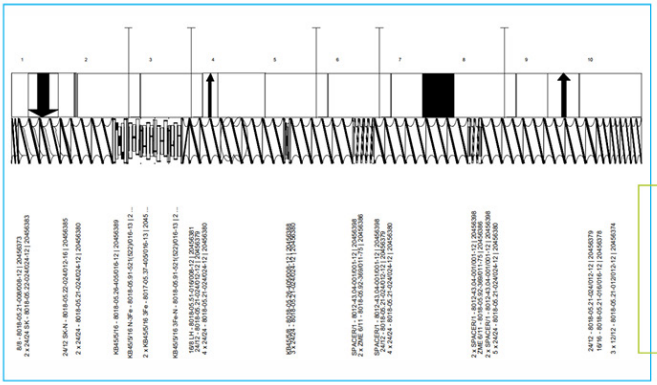

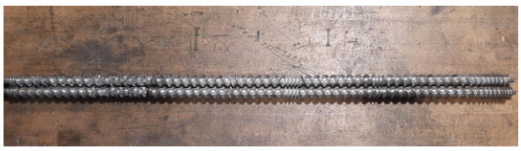

7

4. Compoundage du volume hétérogène

- Paramètres d'extrusion :
  - Rampe de température =>
  - Insertion de la matière manuellement à l'aide de gobelet
  - Débit : 3 kg/h
  - Vitesse : 250 tours/min

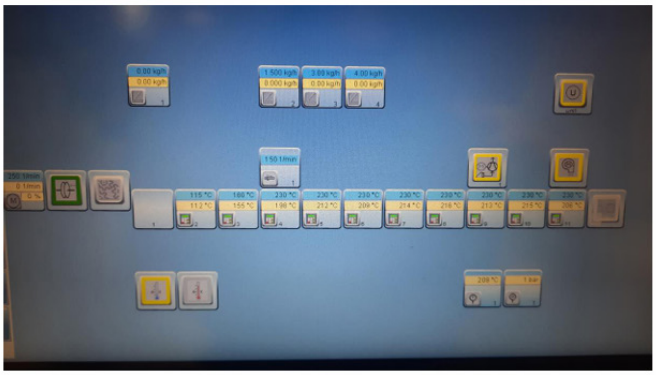

4. Compoundage des volume hétérogènes

- Matière en sortie : PP CF40 %

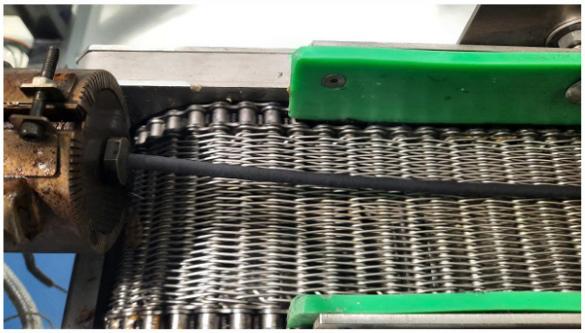

- Matière en sortie : Poly A - CF 40%

Polymère A très fluide => texture plus rugueuse

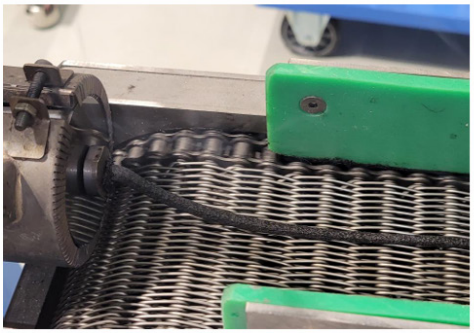

9

4. Compoundage des volumes séparés PP CF

- Débits

Données			
Masse de tape	M_tape	0.414	kg
Masse de PP	M_PP	0.284	kg
Masse totale	M_tot	0.698	kg
Débit masse total	m_point_tot	3	kg/h
Fraction volumique fibre	v_f	0.47	-
Masse volmique tape	rho_tape	1310	kg/m³
Masse volumique PP	rho_PP	910	kg/m³
Masse volumique carbone	rho_carbone	1800	kg/m³
Masse tape/gobelet	M_tape/gobelet	0.04	kg

Calculs				
Volume tape	V_tape	0.00031603	m³	$V_{tape} = \frac{M_{tape}}{\rho_{tape}}$
Volume carbone	V_carbone	0.00014853	m³	$V_{carbone} = V_{tape} \cdot v_f$
Masse de carbone	M_carbone	0.267	kg	$M_{carbone} = V_{carbone} \cdot \rho_{carbone}$
Masse de PP dans le tape	M_PP_tape	0.147	kg	$M_{PP\_tape} = M_{tape} - M_{carbone}$
Masse totale de PP	M_PP_tot	0.431	kg	$M_{PP\_tot} = M_{tot} - M_{carbone}$
Fraction massique carbone tape	m_carbone	0.65	-	$m_{carbone} = \frac{M_{carbone}}{M_{tape}}$
Fraction massique totale carbone	m_carbone_tot	0.38	-	$m_{carbone\_tot} = \frac{M_{carbone}}{M_{tot}}$
Débit massique carbone	m_point_carbone	1.15	kg/h	$\dot{m}_{carbone} = \dot{m}_{tot} \cdot m_{carbone}$
Débit massique tape	m_point_tape	1.78	kg/h	$\dot{m}_{tape} = \frac{\dot{m}_{carbone}}{m_{carbone}}$
Débit massique PP	m_point_PP	1.22	kg/h	$\dot{m}_{PP} = \dot{m}_{tot} - \dot{m}_{tape}$
Débit goblet tape	g_point_tape	44.5	gobelets/h	$\dot{g}_{tape} = \frac{\dot{m}_{tape}}{M_{tape/gobelet}}$
		0.74	gobelets/min	

10

4. Compoundage des volumes séparés

- Bourrage de la fibre
  - Volume de PP a été extrudé plus rapidement que le volume de tape
  - Il restait 30% de la masse initiale de tape, soit 120g
  - Fin du procédé avec 80g de PP de purge
  - Matière obtenue : PP CF30

11

5. Injection

- Conditions d'injection :

Matière	T buse injection [°C]	T moule [°C]	Débit d'injection [cm³/s]	Point de commutation [cm³]	Temps de maintient[s]	Temps de refroidissement [s]
PP CF40 (réservoir recyclé)	230	40	30	3.8	18	40
PP CF30 (réservoir recyclé)	230	40	30	4.5	18	40
PP Purge (sans charge)	230	40	30	3.8	20	40
Pol A-CF40 (réservoir recyclé)	315	120	60	3.8	5	40
Polymer A 5s	315	120	60	3.8	5	40
Polymer A 15s	315	120	60	3.8	15	40

12

5. Injection

- Etudes de remplissage PP CF40

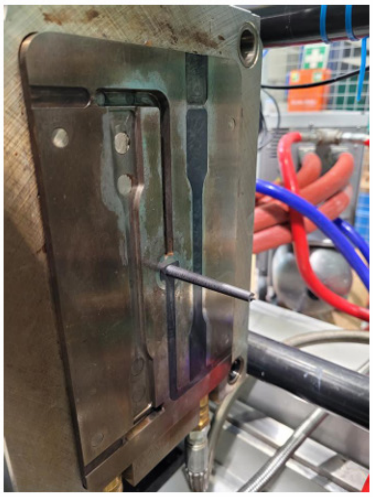

13

6. Essais de traction

- Essais selon la norme DIN EN ISO 527-2/1A/10
- Vitesse de traction : 10mm/min
  - Contraintes maximales
  - Allongements maximaux
  - Modules élastiques

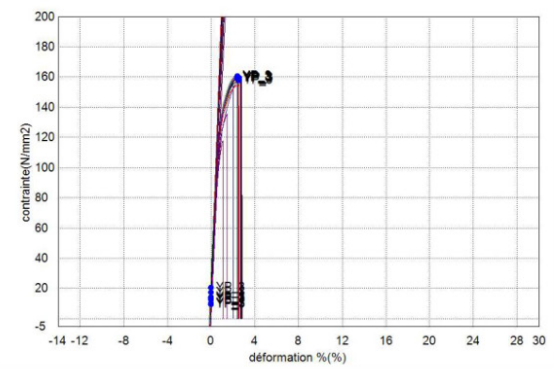

Contrainte/déformation compound polymer A - CF

14

6. Résultats pour les réservoirs en Carbone + PP

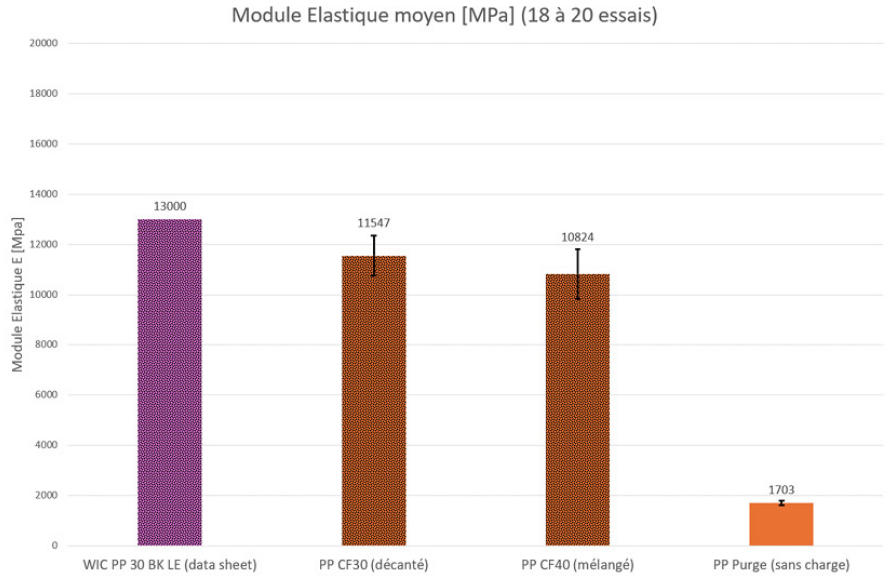

15

6. Résultats pour les réservoirs en Carbone + PP

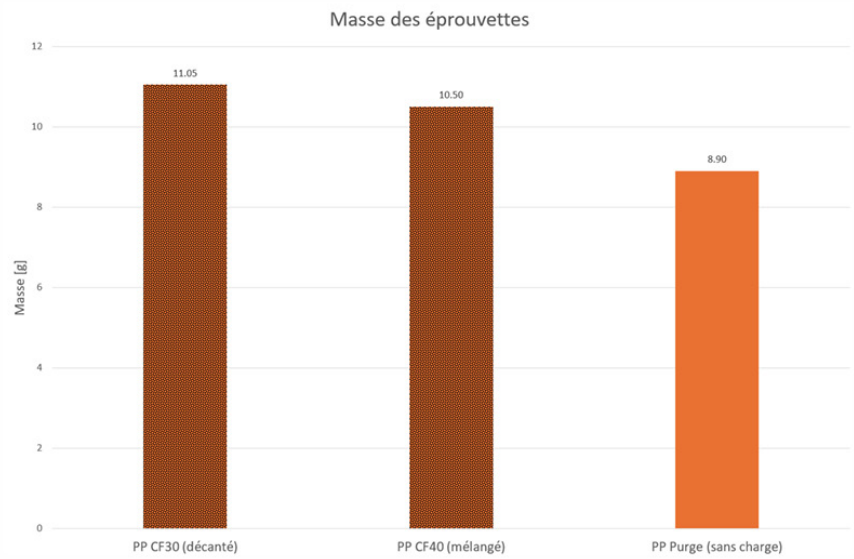

PP CF30 +5% de masse

16

6. Résultats pour les réservoirs en Carbone + PP

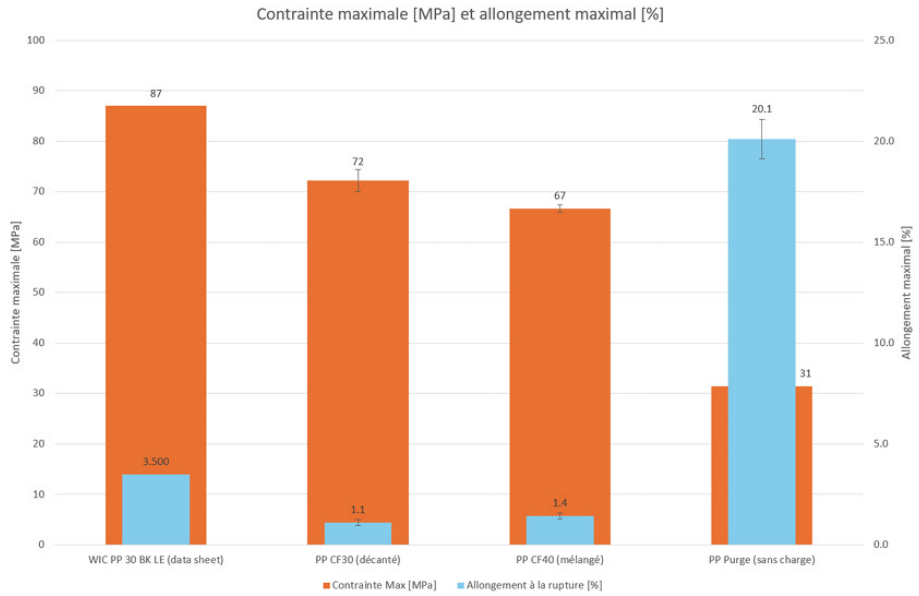

17

6. Résultats pour les réservoirs en Polymère A - CF

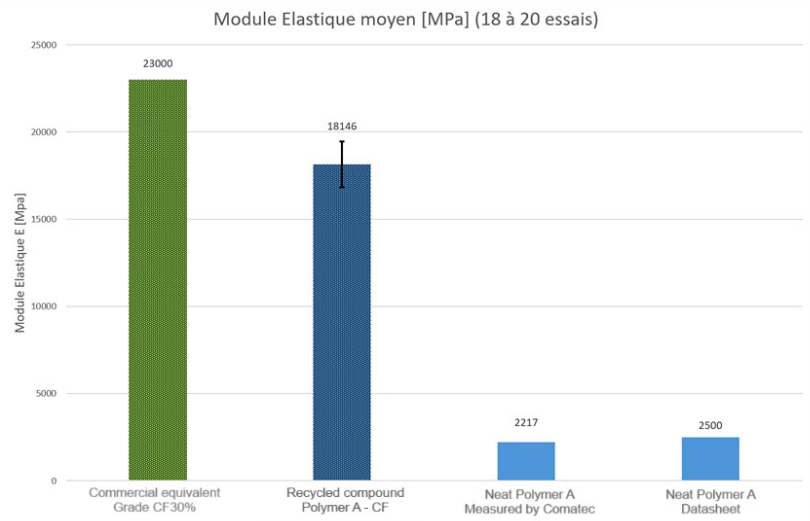

18

6. Résultats pour les réservoirs en Polymère A - CF

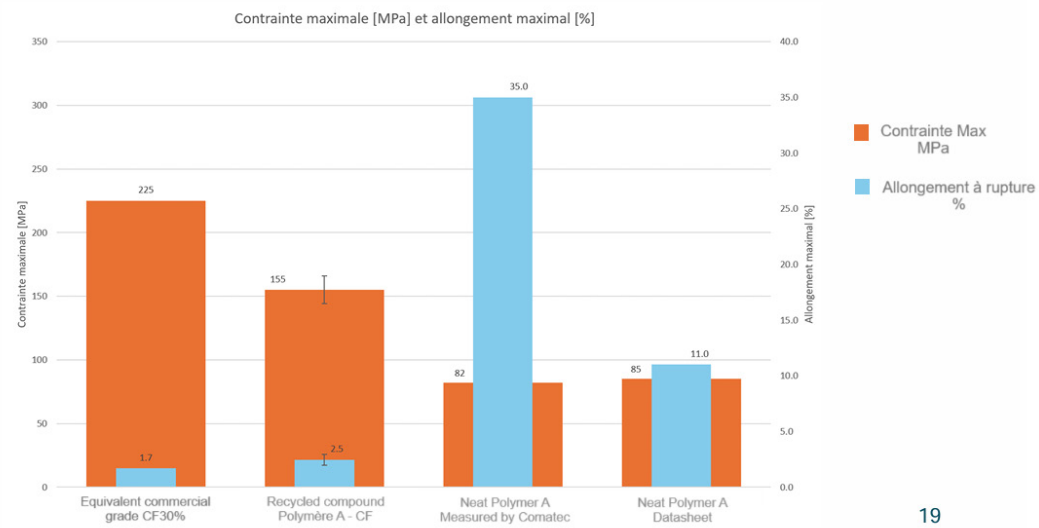

19

6. Conclusions

- Le recyclage des deux types de réservoir est possible
- Pour les réservoirs en carbone + PP, la décantation n'offre pas de réel avantage à ce stade
- Il est possible d'obtenir des propriétés comparables à des matériaux commercialisés
- Avec plus de matière à recycler (5 à 10kg), les conditions d'injection et les propriétés mécanique peuvent être améliorées

20